Journal of
Instrumentation

PAPER • OPEN ACCESS

Technological development and qualification of the HEPD-02 apparatus on board the CSES-02 satellite

To cite this article: S. Bartocci *et al* 2026 *JINST* **21** P11009

View the article online for updates and enhancements.

You may also like

- Solar Wind Anomalies at 1 au and Their Associations with Large-scale Structures
Yan Li, Shaosui Xu, Janet G. Luhmann et al.
- PHOTOCHEMISTRY IN THE INNER LAYERS OF CLUMPY CIRCUMSTELLAR ENVELOPES: FORMATION OF WATER IN C-RICH OBJECTS AND OF C-BEARING MOLECULES IN O-RICH OBJECTS
Marcelino Agúndez, José Cernicharo and Michel Guélin
- Control and read-out of the HEPD-02 tracking system onboard CSES-02 satellite
S. Bartocci, R. Battiston, S. Beolè et al.

This content was downloaded from IP address 93.49.143.230 on 13/11/2026 at 04:33

Published by IOP Publishing for Sissa Medialab

Received: *August 13, 2026*
Accepted: *October 19, 2026*
Published: *November 6, 2026*

Technological development and qualification of the HEPD-02 apparatus on board the CSES-02 satellite



The CSES-Limadou Collaboration, HEPD-02 team

S. Bartocci,[a] **R. Battiston,**[b,c] **S. Beolè,**[d,e] **F. Benotto,**[e] **P. Cipollone,**[f] **S. Coli,**[e] **M. Comelli,**[g] **A. Contin,**[h,i] **M. Cristoforetti,**[j,c] **C. De Donato,**[f] **C. De Santis,**[f] **A. Di Luca,**[j,c] **F. Dumitrache,**[e] **F.M. Follega,**[b,c] **S. Garrafa Botta,**[e] **G. Gebbia,**[c] **R. Iuppa,**[b,c] **A. Lega,**[j,c] **M. Lolli,**[i] **M. Martucci,**[f] **G. Masciantonio,**[f] **M. Mergè,**[k] **M. Mese,**[l,m] **R. Nicolaidis,**[b,c] **F. Nozzoli,**[c] **A. Oliva,**[i] **G. Osteria,**[m] **F. Palma,**[f] **F. Palmonari,**[h,i] **B. Panico,**[l,m] **S. Perciballi,**[b,c] **A. Parmentier,**[p,f] **F. Perfetto,**[l,m] **A. Perinelli,**[b,c] **P. Picozza,**[n,f] **M. Pozzato,**[i] **E. Ricci,**[c] **L. Ricci,**[b,c] **M. Ricci,**[f,o] **S.B. Ricciarini**[g,*] **M. Rinaldi,**[k] **Z. Sahnoun,**[n,f] **U. Savino,**[d,e] **V. Scotti,**[l,m] **E. Serra,**[c] **M. Sorbara,**[n,f] **A. Sotgiu,**[f] **R. Sparvoli,**[n,f] **P. Ubertini,**[p] **V. Vilona,**[j,c] **S. Zoffoli**[k] **and P. Zuccon**[b,c]

[a] *INFN — AC, V. E. Fermi 54, Frascati (RM), 00044, Italy*
[b] *University of Trento, V. Sommarive 14, Povo (TN), 38123, Italy*
[c] *INFN — TIFPA, V. Sommarive 14, Povo (TN), 38123, Italy*
[d] *University of Turin, V. P. Giuria 1, Turin, 10125, Italy*
[e] *INFN — Sezione di Torino, V. P. Giuria 1, Turin, 10125, Italy*
[f] *INFN — Sezione di Roma Tor Vergata, V. della Ricerca Scientifica 1, Rome, 00133, Italy*
[g] *IFAC-CNR, V. Madonna del Piano 10, Sesto Fiorentino (FI), 50019, Italy*
[h] *University of Bologna, V.le Berti Pichat 6, Bologna, 40127, Italy*
[i] *INFN — Sezione di Bologna, V.le Berti Pichat 6, Bologna, 40127, Italy*
[j] *Fondazione Bruno Kessler, V. Sommarive 18, Povo (TN), 38123, Italy*
[k] *Italian Space Agency, V. del Politecnico, Rome, 00133, Italy*
[l] *University of Napoli "Federico II", V. Cintia, Napoli, 80126, Italy*
[m] *INFN — Sezione di Napoli, V. Cintia, Napoli, 80126, Italy*
[n] *University of Roma Tor Vergata, V. della Ricerca Scientifica 1, Rome, 00133, Italy*
[o] *INFN — LNF, V. E. Fermi 54, Frascati (RM), 00044, Italy*
[p] *INAF-IAPS, V. Fosso del Cavaliere 100, Rome, 00133, Italy*

E-mail: sergiobruno.ricciarini@cnr.it

[*] Corresponding author.

© 2026 The Author(s). Published by IOP Publishing Ltd on behalf of Sissa Medialab. Original content from this work may be used under the terms of the Creative Commons Attribution 4.0 licence. Any further distribution of this work must maintain attribution to the author(s) and the title of the work, journal citation and DOI.

https://doi.org/10.1088/1748-0221/21/11/P11009

2026 JINST 21 P11009

Abstract: The China Seismo-Electromagnetic Satellite (CSES) project is aimed at developing a satellite constellation dedicated to the measurement of electric and magnetic fields, plasma currents and particle fluxes in the terrestrial magnetosphere. The first satellite in the series, CSES-01, was launched in 2018 and is still operational. The second satellite, CSES-02, was successfully launched into orbit on 14 June 2025. Within this framework, the Italian Limadou collaboration developed the High-Energy Particle Detector (HEPD) for both missions.

This article focuses on the technological development and qualification of the HEPD-02 apparatus, operating on board CSES-02. HEPD-02 is composed of various scintillator detectors and a pixel direction detector, aimed at measuring the energy spectra of charged particles, either incoming or trapped in the terrestrial magnetosphere. It is optimized for the identification of individual electrons with kinetic energies in the range between 3 and 100 MeV, and of protons between 30 and 200 MeV. This paper illustrates instrument and electronics design, outlining the main technological challenges and adopted solutions to ensure the desired operation and performance in the space environment for the expected lifetime of at least 6 years. It also describes the test campaign which was carried out to demonstrate the fulfilment of mechanical, thermal and electromagnetic requirements.

Keywords: On-board space electronics; Space instrumentation; Calorimeters; Particle tracking detectors

2026 JINST 21 P11009

Contents

1 Introduction **1**

2 The CSES satellites **2**

3 HEPD-02 concept and science **2**

4 The HEPD-02 apparatus **3**
4.1 Instrument assembly 5
4.2 Electronics assembly 8

5 HEPD-02 design: technological challenges and solutions **11**
5.1 General mechanical and thermal design 11
5.2 Scintillators and PMTs mechanics 14
5.3 Direction detector structure 17
5.4 Electronics assembly design 20

6 HEPD-02 qualification and acceptance campaign **24**
6.1 Mechanical stress tests 25
6.2 Thermal and vacuum tests 28
6.3 Electromagnetic compatibility (EMC) tests 29

7 Conclusions **35**

2026 JINST 21 P11009

1 Introduction

This paper presents the system-level technological development and qualification of the HEPD-02 apparatus, operating on board the CSES-02 satellite. It focuses on the design choices to meet the mechanical, thermal, electromagnetic and space-environment constraints of the mission, and on the qualification campaign of the complete instrument for operation on board CSES-02. It complements previous publications dedicated to the description of individual sub-systems, by discussing the technological solutions adopted at system level and the verification of their compliance with the mission requirements.

Section 2 introduces the CSES satellites, in particular CSES-02.

The concept and science of HEPD-02 are briefly described in section 3.

Section 4 contains a general description of the instrument and electronics of HEPD-02.

Section 5 outlines the most significant technological challenges faced and the solutions adopted for the development of the HEPD-02 system and for the integration of the various sub-systems.

Section 6 describes the qualification and acceptance test campaign of the assembled HEPD-02 apparatus to verify compliance with launch and operation on board the CSES-02 satellite.

Conclusions are presented in section 7.

2 The CSES satellites

The China Seismo-Electromagnetic Satellite (CSES) mission [1] is a Sino-Italian scientific space collaboration, led by the China National Space Agency (CNSA) and the Italian Space Agency (ASI). Several Chinese and Italian research institutions participate, the latter forming the Limadou Collaboration.

The CSES programme comprises the CSES-01 and CSES-02 satellites, designed for monitoring the variations of electromagnetic fields, plasma parameters and particle populations of the radiation belts in near-Earth space, which may be induced by natural or artificial sources. The fundamental science objectives are the investigation of temporal correlations with high-magnitude seismic events [2], the study of space-weather phenomena [3] and the measurement of fluxes of cosmic rays [4].

CSES-01 was launched in February 2018, carrying 9 scientific payloads, with the High-Energy Particle Detector HEPD-01 [5] developed by the Limadou Collaboration. The satellite is still operational and has exceeded its minimum design lifetime of 5 years.

CSES-02 was launched on 14 June 2025, immediately starting operation, with an expected lifetime of at least 6 years. The satellite carries 11 payloads, including magnetic field detectors, plasma probes, a medium-energy electron detector and two instruments built by the Limadou Collaboration: the Electric Field Detector EFD-02 and the High-Energy Particle Detector HEPD-02. The CSES-02 satellite was developed by DFH Satellite Co., Ltd. (China). It is based on the CAST2000 platform, with a total mass of 900 kg, peak power consumption of 900 W and data storage capacity of 512 Gbyte.

CSES-02 is flying along a Sun-synchronous polar orbit with a period of 94.6 min, at $\sim$ 500 km altitude and with an inclination of 97.4°, thus reaching latitudes in the range ±82.6°. The orbit of CSES-02 is characterized by 180° phase difference with respect to that of CSES-01, in such a way as to maximize the simultaneous field of view of the constellation. For CSES-01 operations are limited at latitudes in the range ±70°, while for CSES-02 all payloads are working along the entire orbit, thus extending the observation capabilities into the polar regions.

During flight, the data generated by payloads are transferred to the satellite storage memory and periodically transmitted to the Chinese ground segment station, managed by the Chinese National Institute of Natural Hazards (NINH). The relevant data are forwarded to the Italian ground segment, located in the Space Science Data Center (SSDC) of the Italian Space Agency.

3 HEPD-02 concept and science

The High-Energy Particle Detector HEPD-02 aims to detect single charged particles incoming from outer space or trapped in the terrestrial magnetosphere. It is capable of particle species identification, energy measurement and determination of incidence direction. It is specifically optimized for electrons in the kinetic energy range between 3 and 100 MeV and protons between 30 and 200 MeV. It is also capable of detecting other nuclei in a kinetic energy range between 30 MeV/nucleon and 200 MeV/nucleon for He and progressively higher for higher-Z ions.

The key target performances are summarized in table 1. The concept and science of the instrument are specifically described in [6], with a preliminary assessment of the angular and energy resolution in the energy ranges of interest for electrons and protons. Additional information on scientific performances will be described in a dedicated future paper.

2026 JINST 21 P11009

Table 1. List of HEPD-02 key target performances.

Parameter	Value
Kinetic energy range (e^-)	3 MeV to 100 MeV
Kinetic energy range (p)	30 MeV to 200 MeV
Angular resolution	$\leq 10°$ (e^-, $E_{kin} = 10$ MeV)
Energy resolution	$\leq 25\%$ (e^-, $E_{kin} = 10$ MeV)

The measurements carried out by HEPD-02 will contribute to several research fields related to astroparticle and space physics, as briefly outlined here.

HEPD-02 will measure the differential energy spectra of cosmic-ray protons and electrons in a partially unexplored energy range, bridging between the low-energy range covered by the Voyager probes [7, 8] and the higher energies studied by the AMS-02 [9] and PAMELA [10] experiments. Additionally, HEPD-02 will contribute to the study of the solar modulation of these spectra, varying according to the $\sim$ 11-year cycle of solar activity.

HEPD-02 will also study solar energetic particles (SEP) events. These are fluxes of high-energy charged particles originating from solar flares and coronal mass ejections, which pose hazards to space missions and human spaceflight and are a key subject of modern space weather research.

HEPD-02 will monitor the long-term and transient variations in the particle population of the radiation belts. These are formed by high-energy electrons and protons trapped in the Earth magnetosphere, which may affect the electronics on board satellites. The CSES-02 orbit crosses both the inner and outer belts, at different latitudes, as shown in [6] figure 6.

HEPD-02 will also identify and study particle bursts related to the precipitation of electrons and protons from the radiation belts. These may be caused by solar activity, lightning, artificial radio emissions, nuclear explosions, volcanic eruptions, or seismic activity [11].

Last but not least, HEPD-02 can also detect gamma-ray bursts (GRBs) and follow their temporal evolution, thus contributing to the characterization of these energetic events, originating in distant galaxies, which are of fundamental importance for astrophysics. The GRB detection functionality was introduced in [6], where the effective on-axis area is presented. It is worth noting that HEPD-02 is sensitive to gamma rays incident from any direction; the off-axis detection efficiency specifically depends on the surrounding structures of the satellite and is currently under study. More information on the GRB detection capability will be provided in future publications.

4 The HEPD-02 apparatus

The HEPD-02 apparatus (figure 1) is made up of an *instrument assembly* and an *electronics assembly*, described in subsections 4.1 and 4.2.

The two assemblies are installed side by side on a base plate and are enclosed by four lateral walls and a top cover, all made of aluminium alloy. The thick base plate constitutes the mechanical and thermally conductive interface with the CSES-02 satellite. The cover houses the interface connectors for power supply, signals and data. The walls and cover are externally treated with black conductive polyurethane coating (LORD Aeroglaze Z307) to maximize radiative thermal exchange with the surrounding satellite structure.

2026 JINST 21 P11009

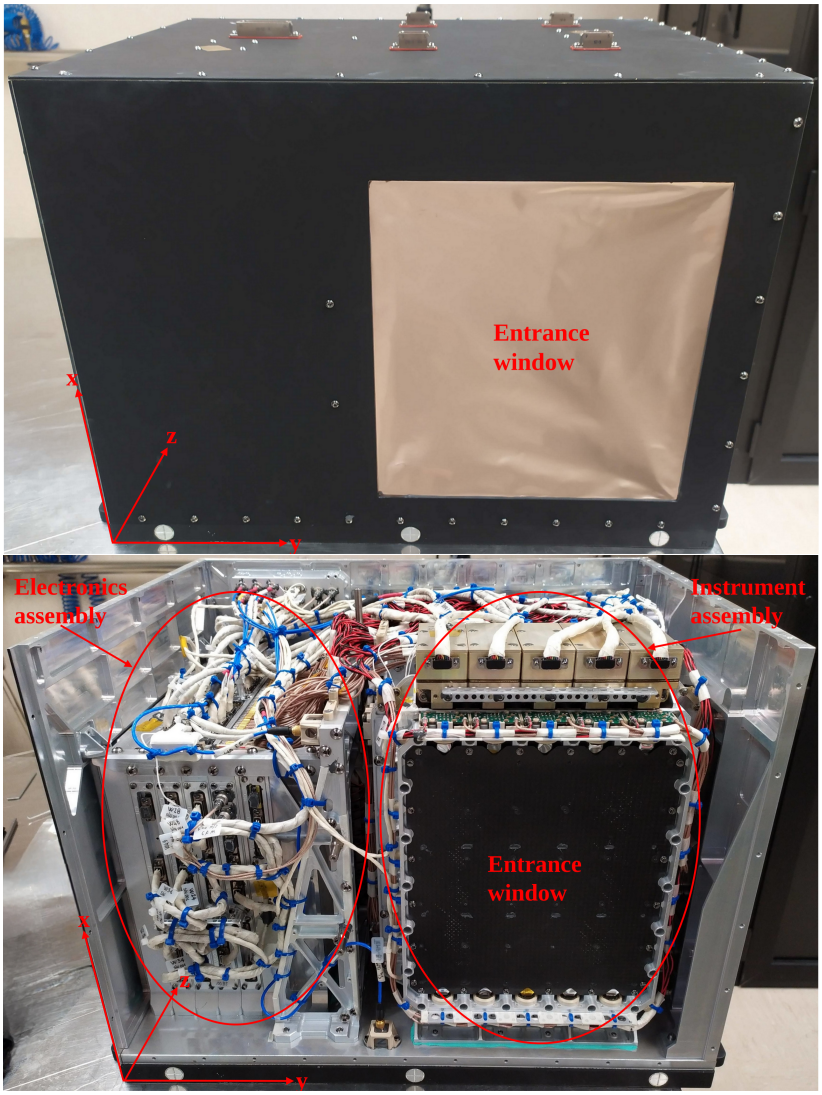

Figure 1. Pictures of the HEPD-02 apparatus. Top: fully assembled. Bottom: opened to show the inside. The xyz dimensions are 37 cm × 53 cm × 39 cm.

The main operational specifications of HEPD-02 are listed in table 2. Compared to HEPD-01, the mechanical, thermal and electrical interfaces with the satellite and the usable volume/mass are unchanged, while the available power has increased by just 5%. The data budget has undergone a major change, from 50 to 100 Gbit/day.

The operation duty cycle has been extended to the entire orbit, while HEPD-01 was kept off at latitudes outside the range ±70°, due to limitations of the satellite power supply. During a few % of the operating time, particle event acquisition is not possible for HEPD-02, mainly because of the dead time corresponding to the processing of single events and the periodic instrument configuration.

On the other hand, the HEPD-02 apparatus contains several innovations and improvements with respect to HEPD-01, with most parts redesigned to increase reliability, introduce new functionalities and improve scientific capabilities. The specific variations are discussed in the following subsections, together with the description of each part of the apparatus.

2026 JINST 21 P11009

Table 2. Main operational specifications of HEPD-02.

Parameter	Value
Operating temperature	−10°C to +35°C
Operating pressure	≤ 6.65 mPa (“vacuum”)
Dimensions (xyz)	37 cm × 53 cm × 39 cm
Mass	47 kg
Max. power consumption	43 W
Data budget	≤ 100 Gbit/day
Lifetime	> 6 years
Operation duty cycle	Full time operational

4.1 Instrument assembly

The instrument assembly (figure 2) is made up of a sequence of sensitive layers and their front-end electronics, stacked along the z axis of the apparatus. During flight, the CSES-02 satellite normally maintains an orientation such that the z axis points to the nadir, thus matching the downward incoming direction of most cosmic-ray particles. For the same reason, the front face of HEPD-02 on the zenith side includes a rectangular opening (see figure 1), where a thin copper-clad polyimide layer (Dupont Pyralux AG) is installed in correspondence with the instrument assembly. This acts as an entrance window for particles, to minimize the amount of material crossed and consequently their interactions before detection.

The first layers encountered by particles incident from the zenith side are the two trigger scintillators, TR1 and TR2, and the pixel direction detector (DIR) between them. These are followed by the thicker calorimeter, formed by the RAN and EN scintillators, where the particles release most of their energy. Bottom (BOT) and lateral (LAT) containment scintillators allow the tagging of particles that do not stop in the inner layers or do not enter from the zenith side.

4.1.1 Trigger detector

The two trigger detector planes TR1 and TR2 [12] define the standard condition for initiating signal read-out and processing in the instrument, namely an incoming particle has to generate signals high enough in both layers to pass the corresponding trigger thresholds. Compared to the single trigger plane of HEPD-01, this double layer allows limiting the read-out to mostly events with the incoming particle trajectory directed towards the underlying calorimeter, with great advantage in terms of scientific quality of collected data.

The trigger planes are made of Eljen EJ-200 plastic scintillator, characterized by a fast rise time (0.9 ns) and a short decay time (∼ 2.1 ns) of the signal. TR1 is 2 mm thick and segmented into 5 bars of dimensions 32.5 mm × 154.5 mm. TR2 is 8 mm thick and segmented into 4 bars of dimensions 36 mm×150 mm, directed perpendicularly to the bars of TR1. As for all HEPD-02 scintillator elements, each bar is enveloped by a thin (23 µm) aluminized mylar foil, to implement adequate optical isolation.

The TR1 bar thickness is set to 2 mm only, in such a way as to minimize both the energy loss and multiple Coulomb scattering of highly-ionizing particles at the lower end of the energy range of interest (see table 1). These particles can then cross the direction detector and reach TR2 for coincidence triggering.

2026 JINST 21 P11009

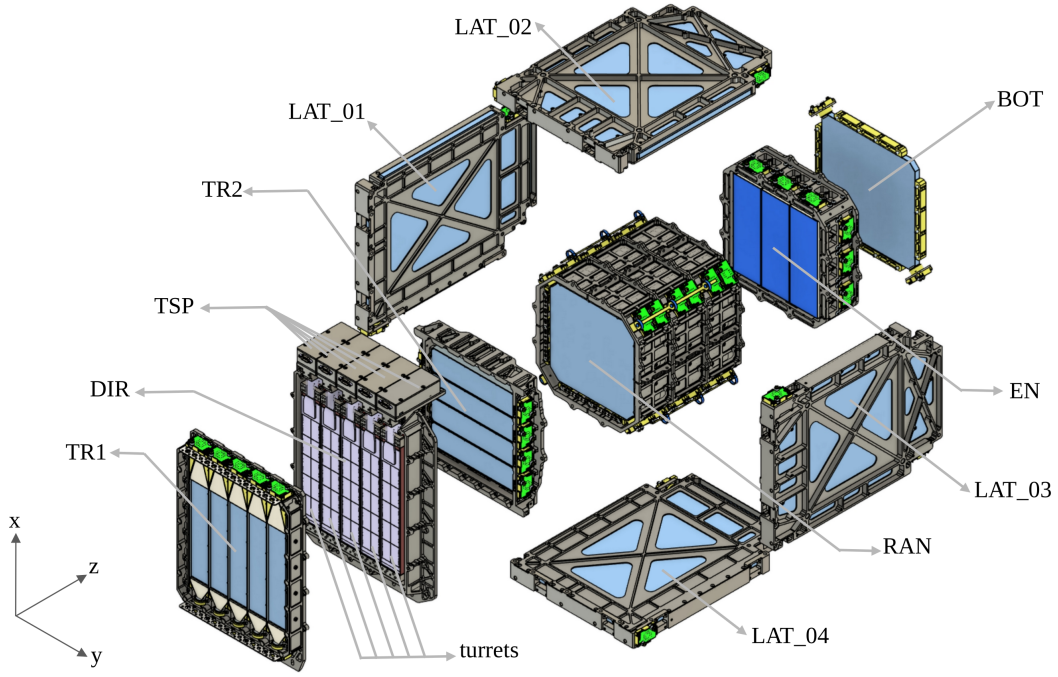

Figure 2. Exploded view of the detectors composing the instrument assembly. During flight, the z axis is kept pointing to the nadir. The compacted assembly xyz dimensions are 33 cm × 28 cm × 38 cm.

For each scintillator bar, the read-out is performed by two photomultiplier tubes (PMTs) placed at opposite ends. The PMT is mounted on a front-end board that receives the externally generated bias voltage and delivers the PMT output signal.

The selected Hamamatsu R9880-210 PMT is a compact and lightweight device, suitable for the small available volume. Its response is fast (2.7 ns transit time) and matches the EJ-200 scintillation timing. It has a high quantum efficiency (almost 40%) in the wavelength region of the maximum emission of the scintillators (~ 420 nm). Its high gain is adjustable in the range between 0.5×10^6 and 3×10^6, to match the light yield of the different scintillator elements used in HEPD-02.

The same PMT read-out scheme is applied to all the other HEPD-02 scintillator elements, as discussed in the following subsections.

4.1.2 Direction detector

The direction detector (DIR) [13], hereafter referred to as the *tracker*, is formed by 5 adjacent *turrets*. A turret (see figure 3) is made up of three superimposed *staves*, equipped with monolithic active pixel sensor (MAPS) devices.

The MAPS used is the Tower Semiconductor ALTAI device, an updated version of the ALPIDE chip [14]. It is characterized by a thickness of 50 µm and an area of 15 mm × 30 mm. It has 512 × 1024 pixels of size 29.2 µm × 26.9 µm. In an ALTAI device, the internal logic identifies the pixels that collected an electron charge exceeding a tunable threshold; their address is recorded and transmitted, thus allowing the identification of clusters of pixels corresponding to particle crossings.

Each stave contains an arrangement of 2 × 5 ALTAI devices with a flexible printed circuit (FPC) glued on top of them. The FPC provides routing for power, bias and digital signals, connected to the chips via triple-redundancy wire bonds. A lateral tracker splitter board (TSP) constitutes the turret

2026 JINST 21 P11009

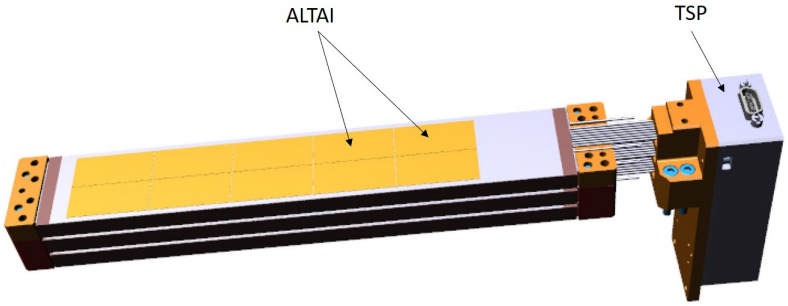

Figure 3. Drawing of a tracker turret, with the FPC of the top stave removed to show the 2×5 ALTAI devices. The TSP board is enclosed in an aluminium box.

interface for the incoming power and for data exchange with the control and read-out electronics. The tracker contains a total of 150 ALTAI chips, corresponding to $\sim$ 80 Mpixels.

It is worth mentioning that the TR1 and tracker detectors are tightly packed together, with a matching sensitive area and segmentation into 5 bars and 5 turrets, respectively. By such a pairing, most particles that give a signal in TR1 also enter the tracker active area for appropriate tracking.

The HEPD-02 pixel tracker represents a remarkable evolution from HEPD-01, which featured two layers of double-sided silicon microstrip sensors. The advantages are a high spatial resolution of $\sim 4\,\mu$m with a noise rate as low as 10^{-10} fake hits/pixel/event. Moreover, the MAPS allows high compactness, since the whole signal processing chain (hit detection, data formatting and compression, digital output) is built inside. In addition, the 3 layers allow redundancy of tracking information.

4.1.3 Calorimeter

The calorimeter implements the measurement of the particle kinetic energy and is composed of two different sub-detectors. Particles incident from the zenith side first enter the range sub-detector (RAN), formed by 12 planes of EJ-200 scintillator. Each layer has thickness 10 mm and area 150 mm$\times$150 mm; it is read-out by two PMTs placed at opposite corners. Low-energy particles are stopped in the RAN layers, where the assessment of the penetration range provides additional information.

The RAN is followed by the energy sub-detector (EN), composed of two layers of much heavier crystal scintillator, namely cerium-doped lutetium-yttrium oxyorthosilicate (LYSO). Both layers are segmented into 3 bars of thickness 25 mm and dimensions 150 mm$\times$49 mm, along mutually orthogonal directions. Each LYSO bar is read-out by two PMTs placed at opposite ends. Particles reaching LYSO typically produce a much larger light output than those stopping in the RAN sub-detector. Proper optical isolation is ensured by a 150 μm thick layer of black polyethylene tape surrounding the mylar foil that envelopes the LYSO bars.

The HEPD-02 EN sub-detector is an evolution from HEPD-01, which had a single layer of nine square LYSO bricks, 40 mm thick, each with a single PMT positioned on the bottom face. In HEPD-02 the overall thickness of the LYSO is 25% higher, which improves particle containment at higher energies. The HEPD-02 bars, though more massive than the HEPD-01 bricks, can be sustained by a much lighter mechanical frame and therefore allow a reduction of inactive support material; in particular, the spacing between adjacent crystals is reduced from 6 to 1.5 mm.

2026 JINST 21 P11009

4.1.4 Containment detector

The containment detector is made up of a bottom (BOT) and 4 lateral (LAT) layers of EJ-200 plastic scintillator, read-out by PMTs placed at opposite corners. These allow tagging low-quality events, such as triggering particles not fully stopping in the inner detectors, and whose energy measurement can therefore be affected by a significant missing fraction.

Compared to HEPD-01, containment effectiveness is improved by positioning the BOT and LAT layers closer to the inner detectors. This is obtained by reducing the thickness of the support frames as much as mechanically feasible and by a different orientation of the PMTs at the corners of LAT planes.

4.2 Electronics assembly

The HEPD-02 electronics assembly includes the read-out, control and power circuits, configured according to the scheme in figure 4. It is made up of five tightly packed modules, which are positioned on one side of the instrument assembly, as shown in figure 1. Each module houses a specialized functional unit with a variable number of printed circuit board assemblies (PCBAs).

The 5 units are here listed and individually presented in the following subsections: trigger board (TRIG), tracker data acquisition board (TDAQ), data processing and control unit (DPCU), low-voltage power supply (LV-PS) and high-voltage power supply (HV-PS).

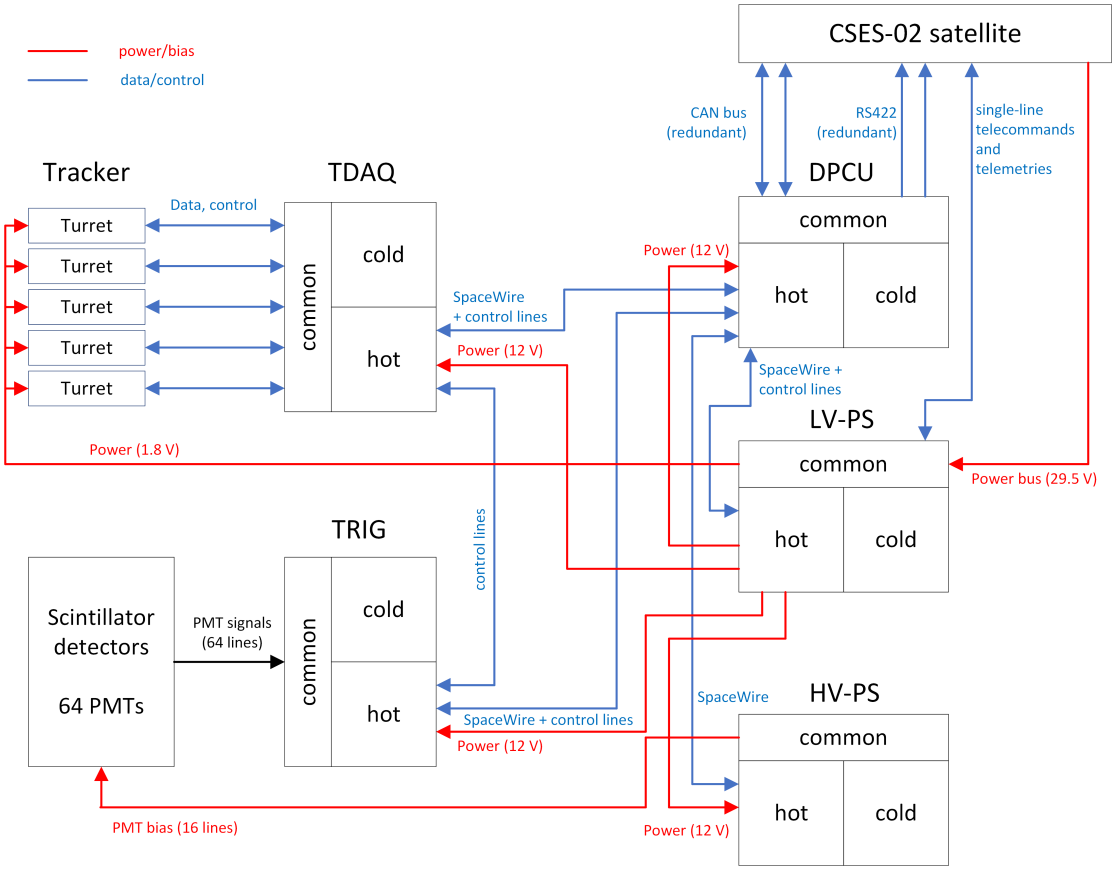

Figure 4. General scheme of HEPD-02 read-out, control and power electronics. The interconnections between cold parts are not shown for better readability; they are identical to those between hot parts.

2026 JINST 21 P11009

The general design is based on the architecture already used for HEPD-01 [15], with the introduction of several substantial innovations and improvements, as described in the following subsections for each unit.

The principle of cold redundancy is adopted for all the units of the electronics assembly, i.e. for each circuit two independent physical copies have been implemented, called hot (or main) and cold (or spare), respectively. Under nominal conditions, the main units are operated while the spare ones are kept powered off; in the extreme case of permanent malfunctioning of the main electronics, the role can be reversed. This solution substantially increases the overall reliability, at the expense of a limited additional design complexity for implementation of appropriate external connections with non-redundant circuits, namely PMT front-ends and tracker turrets.

4.2.1 TRIG

The trigger board (TRIG) [16] processes the signals coming from the 64 PMTs of HEPD-02, which are distributed among the trigger detector, the calorimeter and the containment detector. It performs the measurement of pulse amplitudes and the generation of the instrument trigger signal, needed to start and synchronize the data acquisition of all HEPD-02 detectors. The board also produces the measurement of the live and dead time of the instrument between subsequent triggers.

A MicroSemi ProASIC3E FPGA manages the board operation, with the read-out of the 64 PMTs managed by two Weeroc Citiroc 1A ASICs. A given channel is equipped with two parallel signal processing lines, including a voltage amplifier with programmable gain: from 1 to 60 for the first, from 10 to 600 for the second. Each amplifier is followed by a shaper and a peak detector whose analog output is digitized by an external ADC. A third parallel line is dedicated to generate the logic signal for triggering, raised when the PMT pulse is high enough to represent a particle crossing (a *hit*) in the detector. This line includes a fast shaper (15 ns peaking time) followed by a discriminator with programmable threshold.

The Citiroc 1A was chosen for its wide and adjustable dynamic range, compatible with the variable PMT signal amplitudes characterizing the HEPD-02 scintillator detectors. This variety depends on the different materials and thicknesses of the scintillator elements, and on the variation of light output with the species and kinetic energy of the incoming particle. With respect to the Easiroc device made by the same manufacturer and used in HEPD-01, the Citiroc design has the advantage of a peak detector functionality, which allows measurement of the pulse amplitude without needing an external synchronized sampling signal.

The trigger logic is built inside the FPGA and, compared to HEPD-01, includes the new features of up to 6 concurrent trigger patterns with pre-scaling capability. They give great flexibility for simultaneous acquisition of different particle populations, characterized by different patterns of interactions in the scintillators and different incidence rates. The FPGA also performs a continuous counting of hits, on a second-by-second basis, for single PMT signals and for trigger patterns, thus giving a continuous monitoring of particle rates along the orbit.

4.2.2 TDAQ

The tracker data acquisition board (TDAQ) [17] manages the control and read-out of the direction detector through dedicated digital links with single staves. The board operates the configuration

2026 JINST 21 P11009

and calibration of each ALTAI device, the acquisition of pixel hit maps as a response to a trigger signal, and data exchange with DPCU.

Compared to HEPD-01, the TDAQ board features a completely new design, matching the new concept of MAPS direction detector in HEPD-02.

The TDAQ circuit is based on a Xilinx Artix 7 FPGA, which implements all the required functionalities. The logic structure includes a Microblaze soft processor, used only during the periodic calibration phases for computational tasks, such as determining the optimal pixel hit threshold accounting for noise. The FPGA relies on an external 4-Mbyte SRAM. Two 16-Mbyte flash memories are employed for non-volatile storage of FPGA configuration code and processed data, respectively.

4.2.3 DPCU

The data processing and control unit (DPCU) operates as a general controller of the HEPD-02 apparatus. It manages the interface with the CSES-02 satellite, system configuration and calibration, data acquisition from other units and continuous monitoring of instrument conditions.

The DPCU architecture relies on a Xilinx Zynq XC7Z7045 System-on-Chip (SoC) device, including an FPGA and a dual-core ARM processor. This solution represents an innovation with respect to HEPD-01, where the control and processing functionalities were split between two physically distinct devices, an FPGA and a digital signal processor.

The DPCU operates a redundant RS422 serial connection to transmit the HEPD-02 data to the on-board data handling unit of the CSES-02 satellite, for subsequent downlink to the ground station. The DPCU also manages the slow control interface with the satellite, implemented via a redundant CAN bus channel. It receives telecommands to change the system configuration parameters, or periodic data broadcasts such as absolute time and orbital information. In turn, the DPCU periodically sends back telemetry information on the status of HEPD-02.

Data exchange with the other HEPD-02 units is performed using the SpaceWire Light protocol (IEEE 1355-1995) [18] with individual full-duplex digital connections, with the DPCU acting as master. A burst transfer mode has been introduced in the HEPD-02 architecture, in such a way as to speed up the TRIG and TDAQ read-out. The DPCU performs system diagnostics by periodically checking the status information of the various units. In case of anomaly, it adopts countermeasures depending on the specific condition, such as reconfiguration attempts or safe shut-down of sections of the instrument.

The DPCU automatically configures the active concurrent trigger patterns and pre-scaling values on the TRIG board (see subsection 4.2.1) according to the orbital position. The granularity of this operation is defined by a grid of 128 orbital zones, with 8 longitude cells over $\pm 180^\circ$ and 16 latitude cells covering the satellite range of $\pm 82.6^\circ$.

4.2.4 LV-PS

The low-voltage power supply unit (LV-PS) [19] converts the 29.5 V input voltage of the satellite power bus into lower voltages required to operate the HEPD-02 sub-systems. The LV-PS also manages single-line interfaces with CSES-02, namely telecommand inputs and telemetry outputs. During the initial phases after the HEPD-02 switch-on, the LV-PS performs the controlled power-on of the DPCU. The control and communication functionalities are implemented on a MicroSemi ProASIC3E FPGA.

The main power circuit includes an electromagnetic interference (EMI) filter ECRIM HFH100 and the primary DC/DC voltage converter ECRIM HDCD(20-50)-12-60/SP producing a 12 V output.

2026 JINST 21 P11009

This in turn drives a set of independent supply sections, equipped with fault protection and current sense circuits. They generate 12 V power lines for the other units of the electronics assembly and 1.8 V power lines for tracker turrets.

The LV-PS design constitutes a substantial evolution with respect to HEPD-01. Most notably, the new design introduces a continuous monitoring by the FPGA of the voltages, currents and fault conditions on each power supply section. Moreover, the distribution of 12 V to the other units, instead of a set of voltages below 6 V as in HEPD-01, allows a smaller current flow with corresponding reduction of ohmic drops and mutual interferences.

4.2.5 HV-PS

The high-voltage power supply unit (HV-PS) [19] is dedicated to drive 16 independent bias lines for the 64 PMTs of HEPD-02. The PMTs are grouped in such a way that each two PMTs reading the same scintillator element are connected to different bias channels.

The HV-PS unit is managed by a slow control section based on a ProASIC3E FPGA. Each bias line is adjustable to generate up to ~ 1000 V and driven by a regulated high-voltage supply on a dedicated board (Aerospazio Tecnologie HV3).

Compared to HEPD-01, the HV-PS features an increase in the number of bias channels (from 12 to 16) and a significantly improved power efficiency (from 80% to 90%).

5 HEPD-02 design: technological challenges and solutions

HEPD-02 was conceived as a long-duration experiment in space. Therefore, the main design concern was to achieve complete functional reliability and full compliance with the operational specifications and limitations (see table 2), for the expected lifetime of at least 6 years. This result had to be obtained in the demanding environmental conditions that characterize the orbital flight, and after overcoming the mechanical stresses of the launch phase.

As general design guidelines, the criteria set by ECSS were considered, integrated with the specific experience gained by the Limadou collaboration with the development of HEPD-01.[1]

The following subsections illustrate the most significant aspects of the design of HEPD-02: the general mechanical and thermal features (5.1), the support mechanics for scintillators and PMTs (5.2), the structure of the direction detector (5.3) and the multiple issues concerning the design of the electronics assembly (5.4).

The development and production of HEPD-02 was accompanied by analyses and simulations and supported by laboratory tests of specific parts of the apparatus. After complete assembly, the qualification and acceptance campaign was carried out to verify compliance with mission requirements, as described in section 6. These system-level laboratory tests were of fundamental importance: in fact, the complexity of the structure and the fabrication/mounting tolerances limited the effectiveness of numerical calculations and simulations in taking into account all the mechanical, thermal and electromagnetic details and interactions between the various components.

5.1 General mechanical and thermal design

The structural design of the apparatus underwent radical changes with respect to HEPD-01, following the variations of the instrument layout introduced in subsection 4.1. The new structure had to withstand

[1] ECSS: European Cooperation for Space Standardization, https://ecss.nl/.

2026 JINST 21 P11009

the mechanical stresses applied during test campaign, launch and orbital maneuvers, while propagating low enough stimuli to the fragile parts, i.e. detectors and electronics. A tight control of structural resonance effects was therefore required, specifically avoiding any resonance at low frequencies (< 100 Hz) to prevent counter-thrusts on the satellite structure.

The worst-case stresses to be dealt with were encountered during the mechanical qualification tests (see subsection 6.1): a pyroshock pulse with frequency components in the range between 100 Hz and 4 kHz, with peak acceleration of the order of $1 \cdot 10^3$ g; a sinusoidal stimulus sweep from 10 to 100 Hz, with peak acceleration up to 12 g; a sustained random loading, with spectral contributions from 10 Hz to 2 kHz and overall root mean square (RMS) acceleration of 11.3 g.

Concerning thermal performance, the new design had to ensure proper functionality and stability of materials, interfaces and electronic parts for repeated cycling over a wide field of operating temperatures. These range from -30°C to $+50$°C on the HEPD-02 base plate in the most demanding scenario, i.e. during thermal qualification tests (see subsection 6.2). The implementation of effective heat conduction was required to limit the thermal gradients between the base plate and the rest of the support structure to a few degrees. The design had to take into account the distribution of power-consuming electronic parts and the practical absence of air convection due to the in-orbit vacuum environment ($P \leq 6.65$ mPa).

The creation of a structure with adequate robustness and heat conduction properties was complicated by strict limitations in mass and size (see table 2), which forced the design of relatively compact and lightweight support mechanics. Moreover, the extensive use of steel had to be avoided because of the magnetic cleanliness requirement for installation on board CSES-02 satellite, to avoid interference with the high-precision electromagnetic measurements performed by other payloads.

The general structure of HEPD-02 was developed with successive-approximation design and simulation steps based on finite element analysis (FEA). During the first phase of development, a structural/thermal model (STM) was built to reproduce the general behaviour of the designed apparatus in laboratory tests. This model included the main structural elements, a set of concentrated masses representing heavier components (such as LYSO bars) and resistive loads that emulated the heat produced by electronics. The model was tested for preliminary confirmation of resistance to the pyroshock pulse and absence of resonances with frequencies < 100 Hz.

Subsequently, the design was completed and optimized and the simulations were refined, in particular with the introduction of the finalized layouts of electronics and cabling, bringing more accurate information of heat sources and weights, respectively.

Structural elements of moderate size, such as detectors and electronics support frames, were made of a lightweight and robust aluminium alloy, namely the high-performance space-grade EN AW-6082 (Anticorodal) T651. For larger parts, such as the base plate, external walls and top cover of the apparatus, the need to limit oscillation amplitudes led to the selection of a different alloy, EN AW-7075 (Ergal) T651. This is characterized by higher mechanical strength, at the expense of a lower thermal conductivity, but still acceptable for these specific elements.

Given the non-optimal corrosion resistance of the aluminium, the external surfaces of each element were treated with Surtec 650 V tri-chrome passivation, widely used in space and military applications. This treatment also provided good electrical conductivity of the surfaces, important to avoid the formation of unwanted charge deposits during manipulation.

2026 JINST 21 P11009

The frame elements of the instrument assembly (see figure 5) were structured with surface ribs and thin or missing walls, to save weight; the ribs were dimensioned to achieve the necessary stiffness and thermal conduction. This highly optimized configuration was obtained with a relatively complex, long and expensive design and manufacturing process.

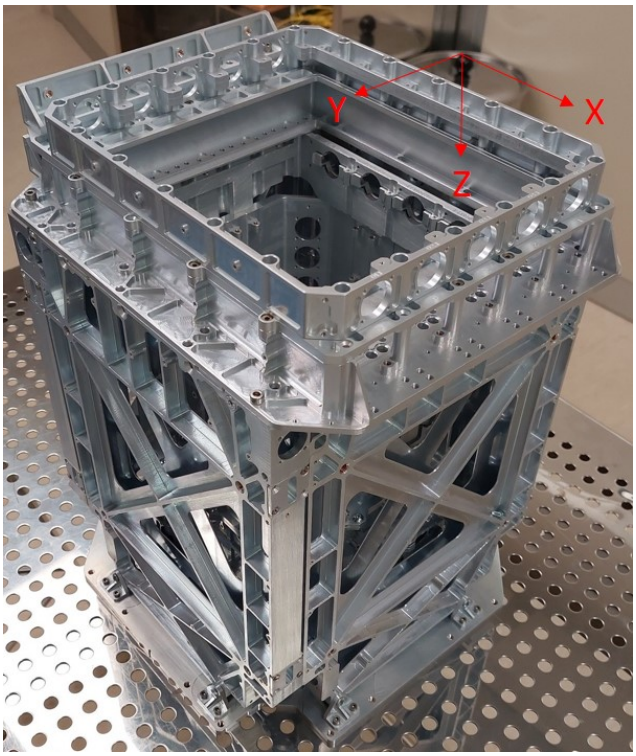

Figure 5. Preliminary stacking of aluminium frame elements of HEPD-02 instrument assembly. The TR1 frame is on top.

Having to discard steel for structural interconnections, Grade 5 titanium alloy was used for screws, washers and column joints to optimize resistance to plastic deformations. Female threads were strengthened by employing wire threaded inserts; since they were not available in titanium, phosphor bronze was selected because of its enhanced corrosion resistance.

A great number of small parts with limited or negligible structural function, e.g. cable holders or PMT support frames, were made of polyether-ether-ketone (PEEK), a high-performance thermoplastic polymer. They were produced by the fused filament fabrication process. This solution gave great advantages over aluminium in terms of reduced weight, variety of obtainable shapes and lower production times and costs.

The low-pressure environment ($P \leq 6.65$ mPa) encountered during flight enhances the outgassing of the materials, which in turn may cause significant adsorption of contaminants on the surfaces. This led to the use of low-outgassing materials that met the ECSS ASTM-E595 standard test method. In addition, the mechanical elements were shaped with adequate ventilation routes (grooves or holes) that avoided the presence of closed volumes in the assembly, where air or gas could be trapped for long periods. Furthermore, the exposed surfaces of PCBAs were generally protected against residual gas contamination by applying low-volatility room-temperature vulcanizing silicone conformal coating (NuSil CV-1152).

2026 JINST 21 P11009

5.2 Scintillators and PMTs mechanics

The support mechanics of scintillators and PMTs in HEPD-02 was redesigned with respect to HEPD-01, due to the substantial variations outlined in subsections 4.1.1, 4.1.3 and 4.1.4.

The general design guideline was kept that the amount (thickness × density) of inactive material, encountered by particles along the z axis (see figure 2), had to be as low as possible to minimize the fraction of energy released outside the scintillators and affecting the measurement accuracy. For such a reason, the support planes on top and bottom of lightweight plastic scintillator elements, namely TR1, TR2, RAN, BOT, were made of carbon fibre reinforced polymer (CFRP), obtained with multiple layers of carbon fibre fabric (GG-160 P) with pre-impregnated composite (IMP 299E). For TR1 and TR2, CFRP ribs were introduced to separate scintillator bars, with the ribs glued between the top and bottom CFRP planes. Figure 6 shows the inner and outer structure of TR1 detector as an example.

Proper mechanical isolation between fragile plastic/crystal scintillator pieces and support mechanics was obtained with interposition of shock-absorbing and vibration-damping materials. For plastic scintillator elements, soft polyurethane foam strips (Rogers Corporation PORON EVExtend 4701-43RL) were used. For the heavy LYSO bars, a much harder padding material was selected, namely silicone gel (TAICA Theta-5).

The design of the TR1 detector was especially demanding, with the TR1 bar thickness reduced to the mechanically challenging value of 2 mm and with the tight packing of TR1 and tracker detectors. In fact, these layout choices introduced several mechanical issues. First, the PMT could not be positioned directly at the end of the TR1 bar to avoid mechanical interference with the underlying tracker frame. Moreover, the very thin and fragile scintillator bars could not be supported by contact with CFRP layers mediated by polyurethane foam strips, as was the case for other scintillator elements. Finally, the cross-section itself of the bar (2 mm × 32.5 mm) did not match the diameter (8 mm) of the PMT photocathode.

The adopted solution was the insertion of light guides made of UV-transparent polymethyl methacrylate (PMMA) at the ends of TR1 bars, as shown in figure 7. Each guide was shaped to optically match the bar cross-section with the PMT photocathode area. The guide length and shape were made different at opposite ends, to match the asymmetric layout of the tracker frame.

The connection of the guide to the end of the bar was stabilized through an indented joint and fixed with optical adhesive (Eljen EJ-500). The bar was therefore suspended between the two guides, which constituted the only contact points with the surrounding CFRP structure. The oscillations of the floating bar were limited by a set of glue points along its length on the adjacent CFRP ribs. The glue was applied through dedicated holes in the top and bottom CFRP planes as the final assembly step. Simulations and laboratory tests showed that the resulting TR1 assembly was strong enough to survive the foreseen mechanical stresses.

Notable innovations were introduced in the design of the mechanical assembly of the 64 PMTs, positioned at opposite ends or corners of each HEPD-02 scintillator element. The assembly is presented in figure 8, while a picture of the actual installation is shown in figure 9.

The optical contact between the PMT input window and the scintillator is mediated through a transparent soft pad (Eljen EJ-560), 3 mm thick, which is kept compressed to ensure a suitable coupling. The PMT has its electrodes inserted and soldered onto a 32 mm × 20 mm front-end board. The board receives the bias (up to ∼ 1000 V from HV-PS) on a twisted-pair line and contains the passive circuit for the distribution of bias to the PMT electrodes. The PMT signal output is sent to

2026 JINST 21 P11009

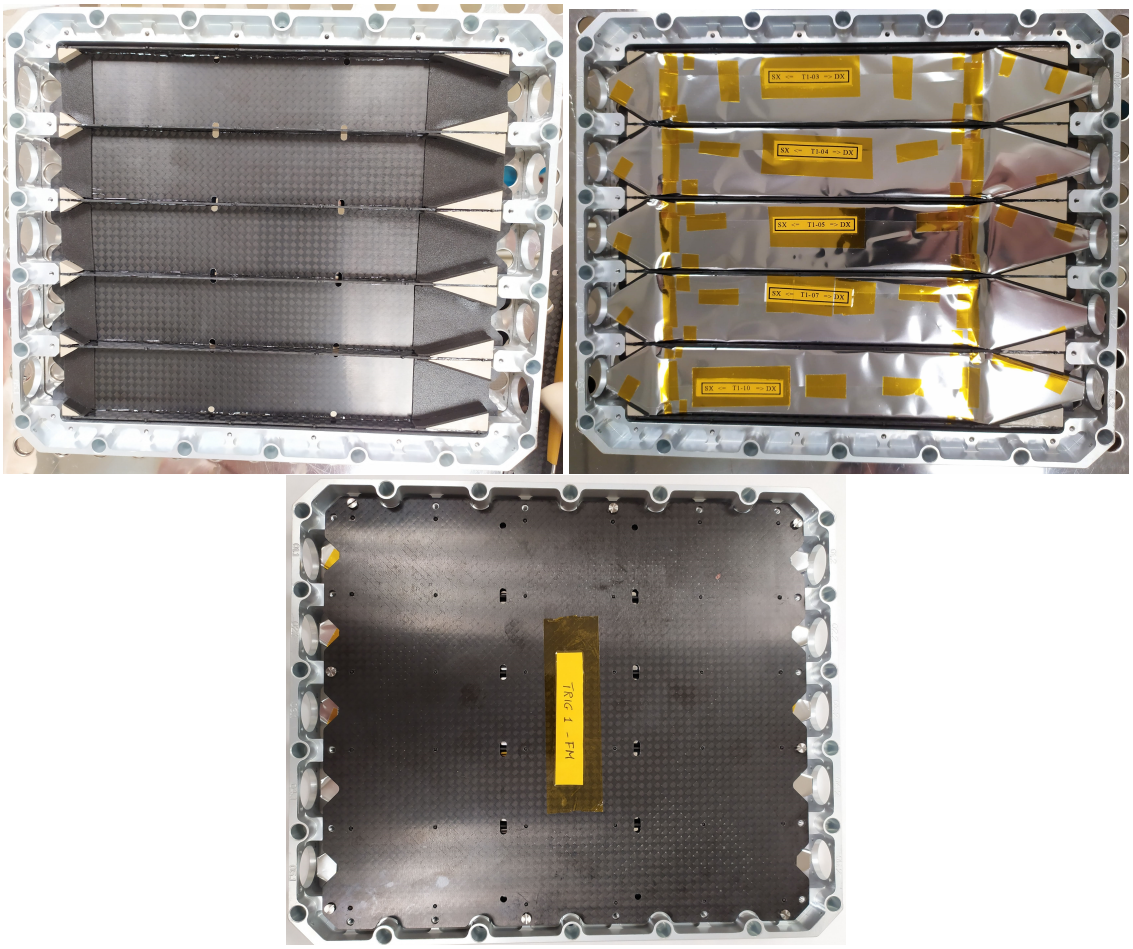

Figure 6. Pictures of TR1 during assembly. Top left: TR1 aluminium frame with CFRP bottom plane and ribs. Top right: TR1 with scintillator bars and light guides in position. Bottom: TR1 completed with CFRP top plane; the holes for application of glue points are visible.

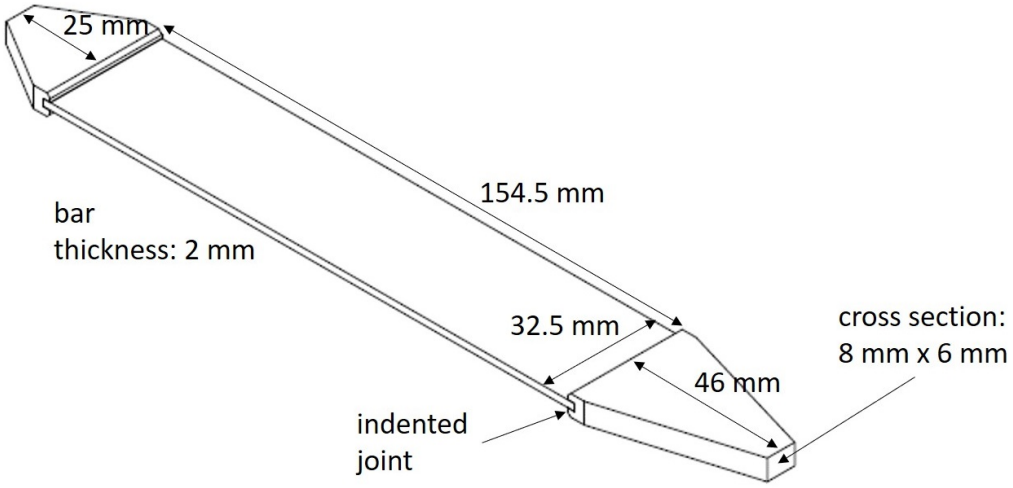

Figure 7. Design of the TR1 bar assembled with light guides.

2026 JINST 21 P11009

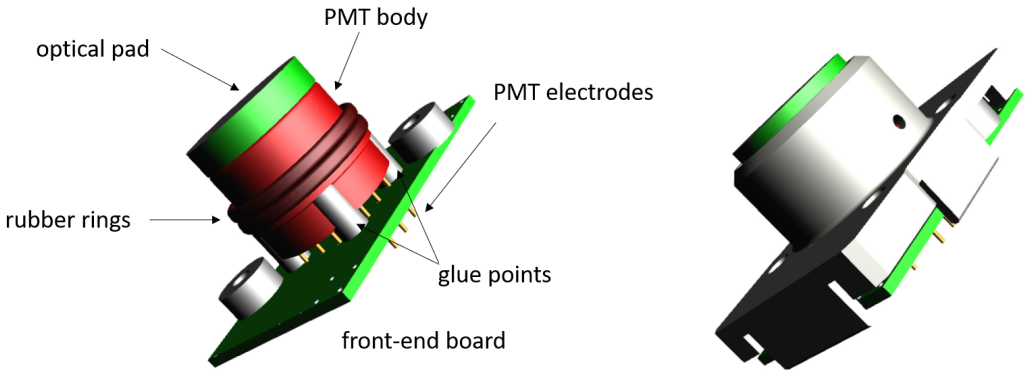

Figure 8. Left: the PMT mounted on the front-end board. Right: the same assembly surrounded by the collar.

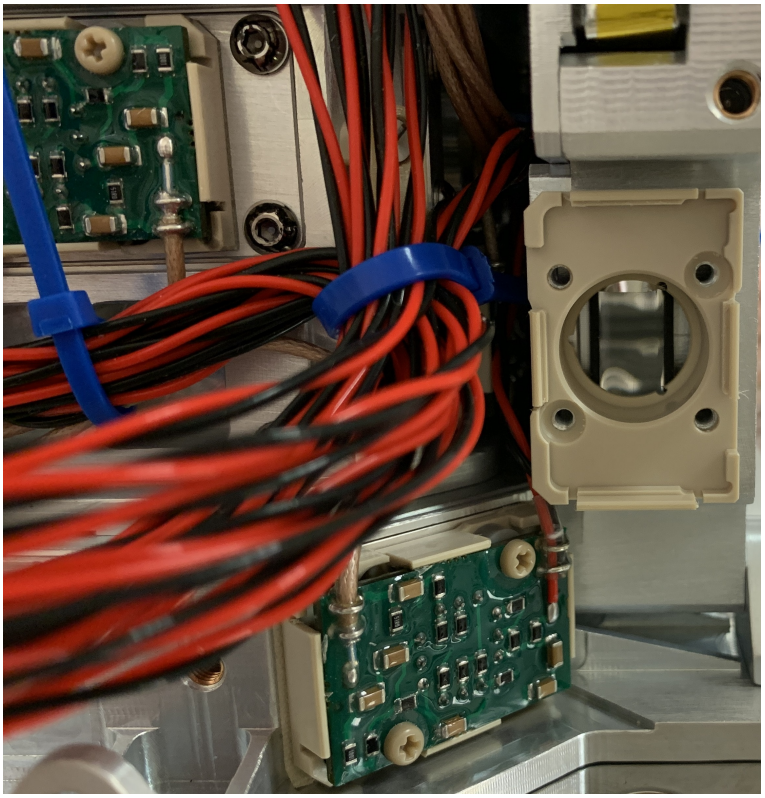

Figure 9. Picture taken during HEPD-02 assembly operations, showing a couple of installed PMT collars with front-end boards and an adjacent collar still without board.

2026 JINST 21 P11009

the TRIG board on a RG 178 coaxial cable (Habia 30000-178-50). The cable was selected for its compactness, with a 1.8 mm external diameter and a 0.3 mm inner conductor diameter, which allows bending and routing in the tight spaces surrounding the small front-end boards.

In HEPD-01, the PMT body was kept in the desired position by directly clamping it with a surrounding collar made of Ultem thermoplastic; the collar was fixed on the scintillator aluminium frame. In HEPD-02, a different approach was used to enhance the protection against stresses and the stability of the optical coupling. The front-end board was fixed by screws on the scintillator frame together with the collar, made of PEEK. In turn, the PMT body was mechanically decoupled from external stimuli driven by the collar, by means of silicone rubber rings. These also compensate for the mismatch between the collar shape and the PMT body due to fabrication tolerances.

Moreover, glue points were applied between the PMT body and the front-end board, to avoid stresses on the PMT electrodes during oscillations of the structure. Finally, the collar was shaped to surround both the PMT body and the corresponding side of the board to increase protection against external contaminating agents, which may form spurious high-voltage discharge paths. This is a fundamental feature, given that for that specific side of the board, typical protections such as coating or encapsulation were not applicable because of the too small spacing.

5.3 Direction detector structure

The direction detector (tracker) was introduced in subsection 4.1.2. It is made up of 5 turrets, each formed by 3 superimposed staves of 2 × 5 ALTAI MAPS. A turret is shown in figure 10, while the general assembly is shown in figures 11 and 12. The HEPD-02 tracker constitutes a completely new design with respect to HEPD-01, with several specific challenges that had to be faced to make it compatible with space flight.

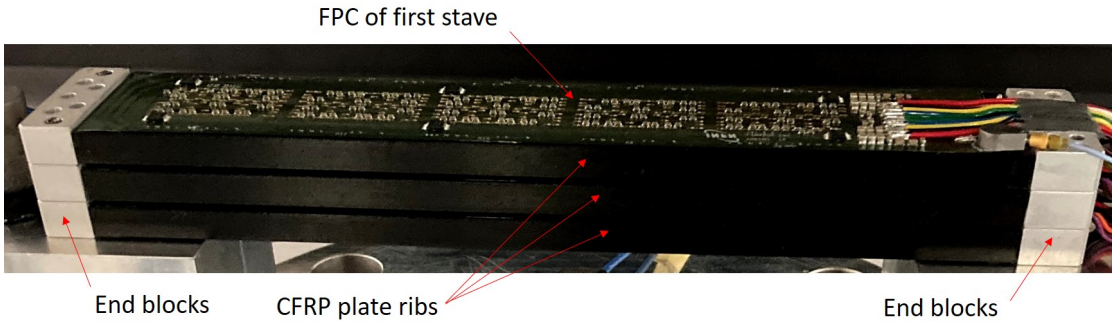

Figure 10. A tracker turret during assembly and test phase.

The thin and fragile assembly of the ALTAI devices with the flexible printed circuit and wire-bond connections had to be housed on an adequately stiff and stable support structure, to withstand the demanding mechanical and thermal stresses expected. Furthermore, the structure had to ensure effective heat conduction towards the HEPD-02 base plate. In fact, the ALTAI device has a maximum allowed operating temperature of +65°C, which is not far from the +50°C reached on the HEPD-02 base plate during thermal qualification tests (subsection 6.2).

The design had also to take into account the opposite requirement of reducing the amount (thickness × density) of inactive material between the ALTAI layers, to limit energy loss and multiple Coulomb scattering of low-energy particles.

2026 JINST 21 P11009

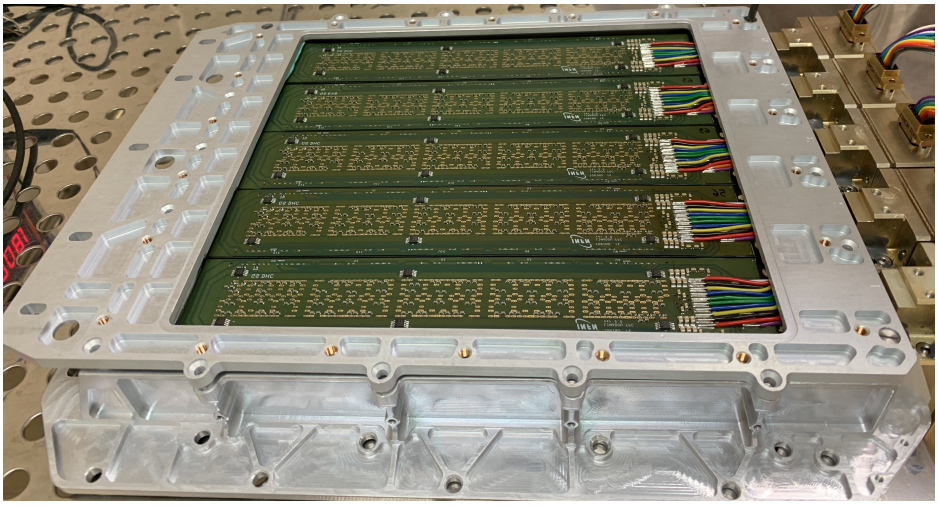

Figure 11. Top view of tracker during assembly operations, with the 5 turrets enclosed in the frame. The 5 flexible printed circuits of the first layer are visible.

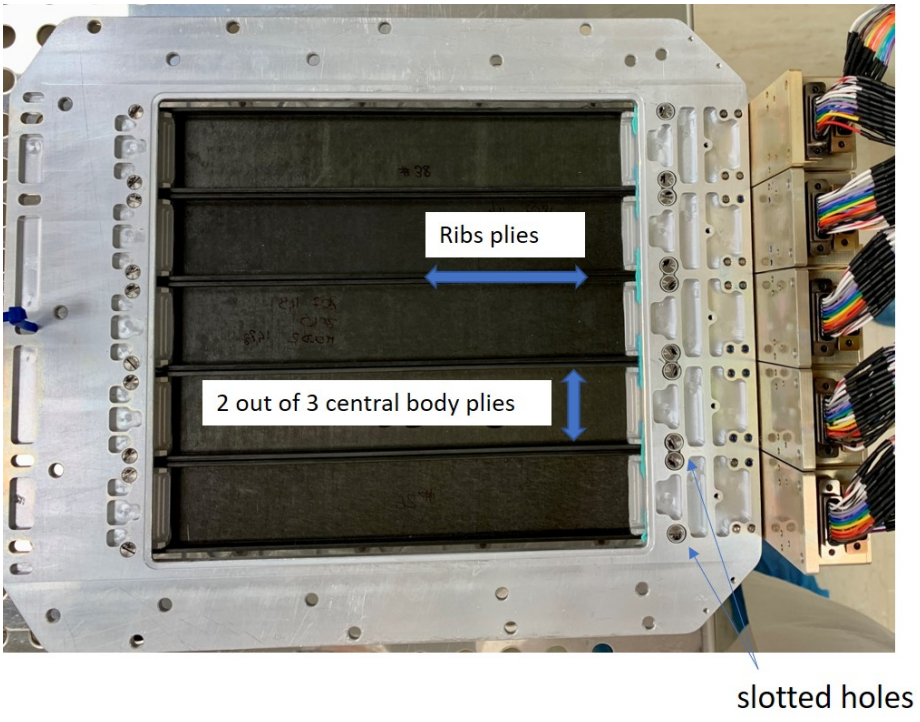

Figure 12. Bottom view of tracker, showing the 5 CFRP plates of the third layer. The directions of the CFRP plies are marked by blue arrows.

2026 JINST 21 P11009

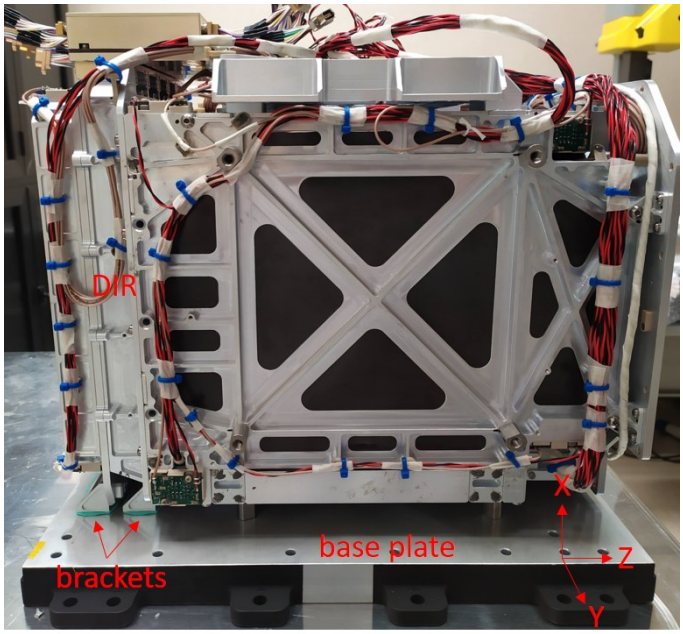

Figure 13. HEPD-02 instrument assembly on the base plate, with a view of the installed brackets for tracker frame.

The above mentioned issues were solved by custom designing a robust and lightweight CFRP plate [20] as a support element for each stave, with the 10 ALTAI devices glued to it using two-component epoxy adhesive (Araldite 2011). The plate was shaped in the form of a C, with a central body and two lateral ribs, made up of several plies of carbon fibres (K13D2U) with cyanate ester pre-impregnated resin (EX1515). The central part consisted of only three fibre plies, for a total thickness of 0.4 mm, to minimize the quantity of material under the ALTAI devices. Two of the three fibre plies forming the central part were directed transversally, while the 14 plies composing each rib were all directed longitudinally. This geometry maximized the thermal conduction from the ALTAI devices to the ribs and then towards the CFRP plate ends.

Each plate end was glued to an aluminium end block. The end blocks of 3 staves were stacked to build a turret; finally, each turret was installed on the tracker frame. The large difference between the thermal expansion coefficients of CFRP and aluminium ($\sim$ 2.5 and $\sim$ 25 ppm/°C, respectively) and the high temperature excursion during environmental tests were taken into account by using a two-component epoxy glue (Masterbond EP37-3FLFAO) best suited to mediate local deformation gradients.

The fixing between the turrets and the tracker frame was made through slightly slotted holes on one end (see figure 12). These gave appropriate tolerances for the different thermal elongations and contractions of the stave assemblies with respect to the frame. The lateral distance between adjacent turrets was set at 0.6 mm to avoid mutual mechanical interference during oscillations of the structure, with the highest amplitude oscillations expected during the HEPD-02 pyroshock test. The spacing thus introduced between the turrets created a small 1.6% inactive area within the detector.

The tracker frame was directly connected to the HEPD-02 base plate with two adjustable brackets (see figure 13). These were tightened after completing the overall assembly, to enhance thermal contact. The thermal conduction between the aluminium parts (end blocks, frame, HEPD-02 base plate) was increased by interleaved pads of high thermal conductivity (Laird Tflex HD80000).

2026 JINST 21 P11009

The absorbed power and therefore the heat produced by the ALTAI devices was limited to fit the direction detector in the power budget of the apparatus. This was obtained by introducing serial read-out of the devices within each stave, by slowing down the data transfer rate and by time gating the clock signal, as explained in [17]. With these solutions, the power consumption was set to ~ 0.5 W/stave, to be compared with ~ 1.5 W/stave of a typical ground-based experimental set-up. The slow-down of data read-out introduced a dead time of a few hundred µs, still compatible with the frequency of the acquisition triggers in HEPD-02, of the order of 400 Hz or lower.

With this overall design, the thermal gradient between the HEPD-02 base plate and the ALTAI devices was limited to less than 7°C, as verified by dedicated measurements under vacuum conditions.

The fulfilment of mechanical and thermal design requirements was preliminarily verified with dedicated tests on single turrets, as discussed in [13] and subsequently with the HEPD-02 system-level test campaign (see subsections 6.1 and 6.2).

5.4 Electronics assembly design

The electronics assembly (introduced in subsection 4.2) includes 5 modules and their cable interconnections, with most PCBAs and cables constituting new designs with respect to HEPD-01. In addition to the already mentioned ECSS design guidelines, the development of HEPD-02 electronics followed the specific high-quality standards stated by IPC.[2]

Mechanics. The modules (see figure 14) were built on robust one-piece aluminium support frames. The PCBAs were tightly fixed to the frames, through a set of screw joints, uniformly distributed in the board area at distances of a few cm, to limit board oscillations that can cause damage to internal tracks and solder joints of surface-mount devices.

Specific actions were taken to protect the solder joints from mechanical damage. The oscillations of bulky parts with respect to the board were limited by applying glue points (epoxy adhesive 3M EC-2216 B/A Gray). Parts with gold plated pins underwent a preliminary *degolding* process by dipping in a solder bath before mounting on PCBA. This treatment avoided gold diffusion into the solder during heating, which can result in fragile joints. All joints were visually and X-ray inspected, to verify the absence of defects. X-ray imaging was the only possible inspection for ball grid array (BGA) parts, whose joints are buried between the device body and the underlying PCB.

The more than 50 interconnection cables for power and digital lines were custom designed and assembled to meet the strict limitations of total weight and available space for routing, at the cost of defining special production and quality assurance procedures. Cable lengths were matched to the defined geometric paths to save mass, and a lightweight and flexible composite thermoplastic braid (Glenair AmberStrand) was selected as the cable screen. The cable structure was mildly stiffened and protected with an external wrapping of glass cloth tape (3M 361).

The Glenair Micro-D MWDM series connectors were used on the power and digital cables; correspondingly the GMR7590 series was mounted on the boards. These connectors are characterized by compactness and high reliability.[3] The body of the board connector was fixed to the frame structure to limit the oscillations and corresponding mechanical stresses applied to the PCBA solder joints.

[2] Global Electronics Association or IPC, https://www.electronics.org/. The general PCBA design in HEPD-02 follows the IPC 6012 Class 3 standard.

[3] Glenair Micro-D connectors comply with U.S. Department of Defense MIL-DTL-83513 military detail specification.

2026 JINST 21 P11009

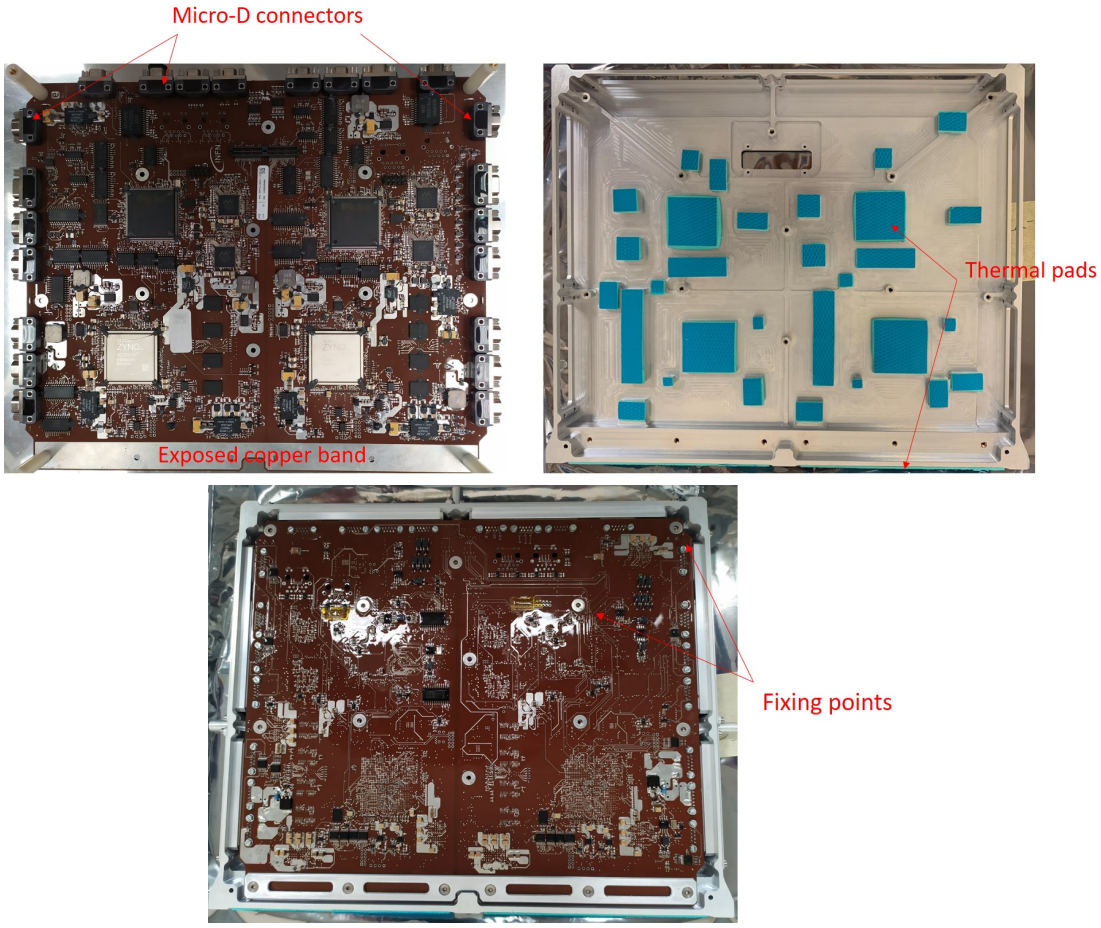

Figure 14. Example of electronics assembly module. Dimensions: 30 cm × 24 cm × 2 cm. Top left: DPCU board main side. Top right: DPCU frame with installed thermal pads on extrusions and on bottom external side for contact with HEPD-02 base plate. Bottom: assembled DPCU module after flipping the board, fixing screws to be inserted.

The 64 coaxial cables delivering the PMT signals to the TRIG board had to face similar limitations in volume and weight. The selection of mini-coaxial connectors (Huber+Suhner MMCX series) allowed the construction of compact and lightweight cables and the positioning of all connections in the available space, on the main edge of the TRIG board (see figure 15). This tight assembly required the design and production of a customized tool to disconnect individual cables during the test phase. The oscillations of the body of the board connector were limited by fixing the coaxial cables on the frame with a clamp bar, also visible in figure 15.

Heat. The structure of the modules (see figure 14) was designed to provide efficient heat removal from the powered components.

The PCB layout included a wide exposed copper band connected to an internal layer that collects heat throughout the entire area of the board; the band was clamped to the underlying support frame in the assembled module. Frame extrusions implemented direct thermal contacts with the most power-consuming electronic parts, mediated by high-conductivity pads (Laird TFlex HD80000). The pad material is soft enough to avoid mechanical stresses on the plastic cases of the parts when the

2026 JINST 21 P11009

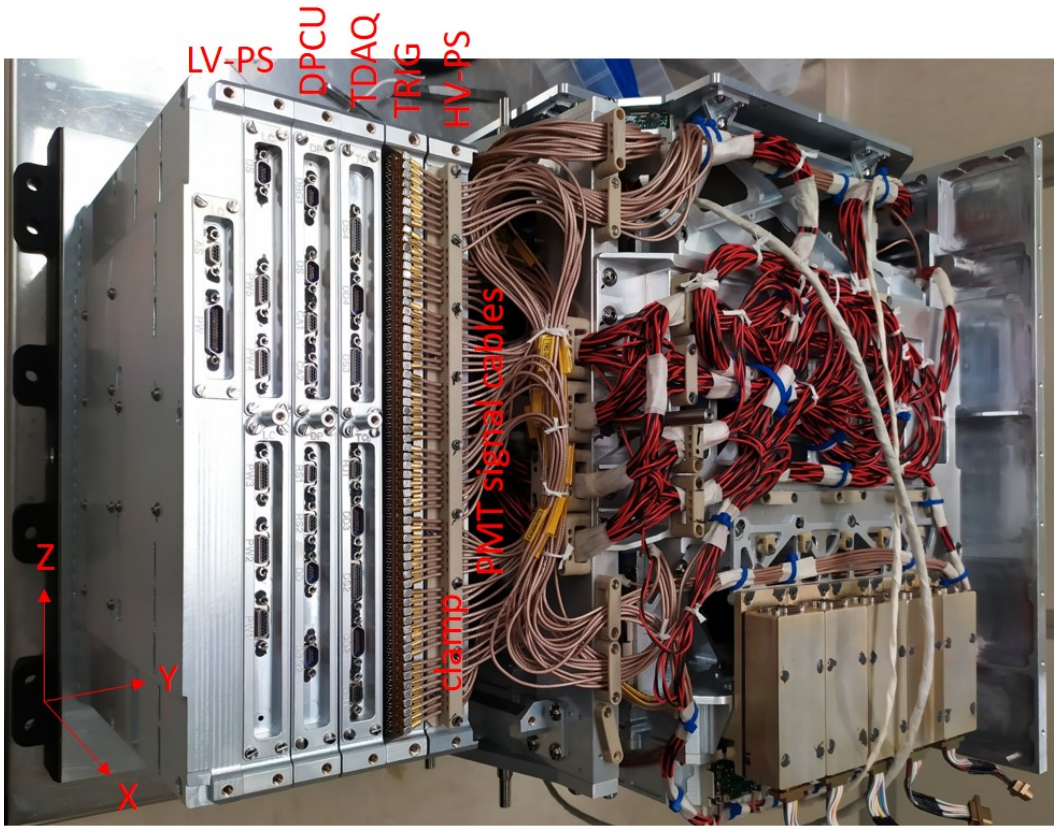

Figure 15. Partially assembled HEPD-02 with the 5 electronics assembly modules installed.

assembly is tightened. The thermal contact between the frame and the underlying HEPD-02 base plate was also enhanced by HD80000 pads.

The maximum temperature reached by the HEPD-02 base plate was +50°C, during the thermal qualification tests (subsection 6.2). The electronic components were therefore chosen with a correspondingly large operating temperature range. Space-qualified parts (−55°C to +125°C) or AEC Q100, Q101 and Q200 automotive-grade parts (−40°C to +125°C) were generally used.[4] For less demanding cases, industrial-grade parts (−40°C to +85°C) were selected.

FEA structural simulations of the apparatus determined the worst-case thermal gradients from the base plate to each power-consuming part, taking into account the distribution of power dissipation on the board areas and the internal layout of each board. For specific power components of the LV-PS unit, the calculated silicon temperature reached more than +85°C, while most of the PCB areas were just a few degrees above the base plate temperature of +50°C. For all parts, the calculated temperature turned out to be at least ∼ 30°C lower than the maximum operating temperature allowed, thus obtaining a wide margin as recommended by ECSS guidelines.

Electromagnetic interferences. The design of the electronics assembly of HEPD-02 had to carefully consider the impact of electromagnetic interferences generated by satellite equipment and other

[4] AEC: Automotive Electronics Council, http://www.aecouncil.com/.

2026 JINST 21 P11009

payloads. Vice versa, electromagnetic emissions from the HEPD-02 circuits could potentially cause disturbances to other HEPD-02 circuits or to the rest of the satellite.

As a measure of optimizing the shielding against radiated interferences, the aluminium frames surround each PCBA on all sides and are connected to the screens of power and digital signal cables. Digital signal cables were generally configured with differential twisted-pair lines to substantially remove ground-related interference and magnetic coupling with other circuits.

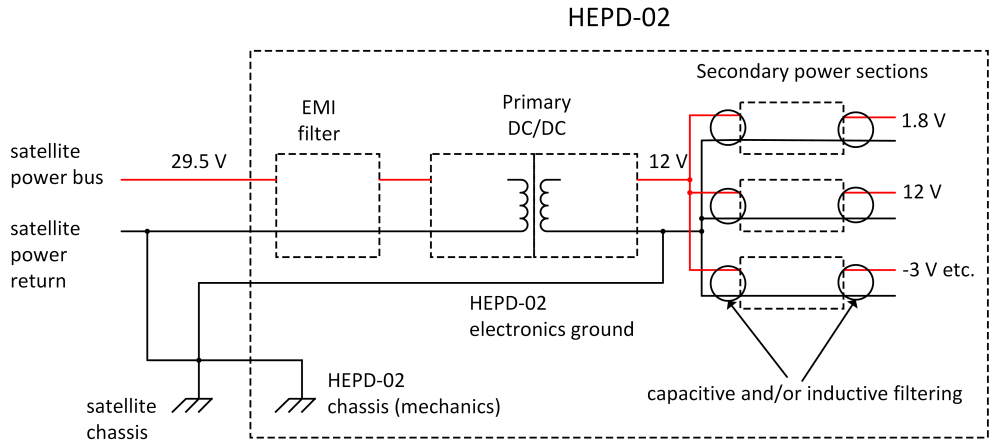

Figure 16. Scheme of power line filtering and electronics ground isolation to minimize conducted interferences in HEPD-02.

Interferences conducted through the satellite power bus were minimized in the LV-PS by the input EMI filter and by the primary DC/DC isolating the electronics ground of HEPD-02 from the satellite power bus return line, as shown in figure 16. Furthermore, the satellite power return, HEPD-02 electronics ground and HEPD-02 mechanics (chassis) were all isolated between each other and short-circuited only in a single physical point of the satellite chassis. This solution avoided DC injection of interferences conducted through the mechanics.

A large part of mutual internal interference is produced by the continuous switching of the secondary DC/DC voltage converters distributed on the various boards. The ripple currents thus generated propagate through the power lines connecting the LV-PS with the other units, potentially affecting circuits at both ends and coupling with nearby signal lines in the tight cable assembly. This source of interference was limited by capacitive and inductive filters (also represented in figure 16) with a band that matched the DC/DC switching frequency.

The effectiveness of the adopted design was experimentally verified with operational tests of the fully assembled apparatus and subsequently with specific electromagnetic compatibility tests for operation in the satellite environment (subsection 6.3). Finally, the actual electromagnetic compatibility was verified after installation on board CSES-02 with the satellite-level test sequence.

Radiation environment. The radiation environment along the CSES-02 orbit is formed by the charged particles trapped in the terrestrial magnetosphere and by those incoming from outer space, with an important contribution from SEP events during periods of solar activity. The effects of the in-orbit radiation were simulated with dedicated tools from the SPENVIS suite.[5]

[5]The Space Environment Information System (SPENVIS): https://www.spenvis.oma.be/.

2026 JINST 21 P11009

To take into account aging due to radiation exposure, electronic parts were chosen among those qualified for a cumulative absorbed dose at least one order of magnitude higher than the $\sim$ 1 krad expected in 6 years of operation. The dose prediction was calculated with the SHIELDOSE tool, by using the SPENVIS standard model for trapped particles and the ESP model for solar protons.[6] In the calculation an average 20 mm equivalent aluminium shielding was assumed, to take into account the satellite and HEPD-02 mechanics surrounding the electronics assembly.

Concerning the risk of single-event effects (SEE) initiated by highly ionizing particles, such as heavy nuclei or low-energy protons, two different selection criteria were applied. On the one hand, the SEE cross sections for events causing local permanent damage (such as MOS transistor gate rupture or CMOS cell latch-up) had to be small enough to imply substantial immunity of parts in 6 years. On the other hand, a limited susceptibility of digital devices to recoverable bit upset events (SEU) was tolerated, for a total expected rate of SEU in the whole HEPD-02 apparatus of few events per year.

For selected critical devices and registers, the effects of SEU were mitigated by introducing automatic error detection and correction (EDAC) through Hamming logic and continuous scrubbing of FPGA configuration memory. Furthermore, the system was configured for prompt reaction to a possible SEU affecting operation. The DPCU periodically performs diagnostic checks of all the units and of their power status, with automatic reaction in case of anomaly. In turn, a possible freezing of the DPCU processor is detected by a watchdog circuit housed in the LV-PS, which triggers a reboot.

6 HEPD-02 qualification and acceptance campaign

Two identical HEPD-02 units were assembled in the clean rooms of the INFN structure of Roma Tor Vergata (Italy): the Qualification Model (QM) and the Flight Model (FM), the latter to be installed on the CSES-02 satellite. These units were subjected to a series of preliminary verifications at room pressure and temperature, addressing the correctness of system operation and the absence of significant effects due to mutual electromagnetic interferences of internal components. Moreover, scientific performances were assessed by means of beam test calibrations and acquisition of cosmic rays at ground level, as described in [6] and in a dedicated future paper.

A sequence of environmental tests followed, in the period between December 2022 and July 2023, to demonstrate that the apparatus was compliant with mechanical, thermal and electromagnetic qualification of the QM and acceptance of the FM. Table 3 shows a synthetic list of these tests, which illustrates the conditions to be verified, the success criteria and the test outcomes. Details will be given in subsection 6.1 for the mechanical stress campaign, in subsection 6.2 for the thermal and vacuum tests, and in subsection 6.3 for the measurements of electromagnetic compatibility.

The test specifications followed the general ECSS guidelines, adjusted to the specific features of the HEPD-02 apparatus and the CSES-02 satellite. Both the qualification and acceptance tests constituted a considerably more challenging use case than expected during the launch and flight phases. The acceptance test conditions were milder to avoid excessive overstress of the FM unit.

All the above mentioned tests were executed for both the main and spare sides of HEPD-02. The incoming flux of high-energy cosmic rays at ground level (mostly muons) allowed a continuous

[6] NASA/TP-1999-209763. Space Environment Effects: Model for Emission of Solar Protons (ESP), M.A. Xapsos et al., 1999.

2026 JINST 21 P11009

Table 3. Synthesis of environmental tests performed on HEPD-02. (*) Found susceptibility to the injected interference levels, which were set conservatively higher than those expected in CSES-02 environment. No susceptibility observed during subsequent satellite-level tests. See subsection 6.3.1. (**) Found emissions levels over the reference thresholds, which were set conservatively lower than the actual susceptibility thresholds of the rest of CSES-02 equipment. Emissions confirmed to be fully acceptable with satellite-level tests. See subsection 6.3.2.

Condition to be tested		**Applied test**	**Success Criteria**	**Test Outcome**
Mechanical stress	Rocket stage separation	Pyroshock	Operation not affected, structure not affected	Passed
	Launch and flight maneuvers	Vibrational stimuli		
Thermal and vacuum	Long-duration, wide-range temperature cycling	Temperature cycles in air and vacuum	Correct operation over the whole range	Passed
Electro-magnetic compatibility	Susceptibility to interferences	Conducted and radiated stimuli	No susceptibility in CSES-02 environment	Passed(*)
	Emission of interferences	Conducted and radiated measurements	Acceptable emission for CSES-02 environment	Passed(**)

particle acquisition even in the absence of particle beams. Until installation on satellite, HEPD-02 was operated through a custom designed electrical ground support equipment (EGSE) emulating the CSES-02 power, control and data interfaces under the control of a PC.

6.1 Mechanical stress tests

These tests were aimed at verifying the ability of the HEPD-02 structure to withstand the mechanical stresses arising during launch and orbital maneuvers. The campaign was carried out in the SERMS s.r.l. laboratory in Terni (Italy) and included pyroshock and vibrational stimuli.

The pyroshock test checked the resistance to the firing of explosive bolts during the separation of the rocket stage from the satellite. The test was performed with the SERMS custom-made Pyroshock Simulator. The shock stimulus was applied in succession along the three axes, twice per axis, to assess the level of repeatability of the shock spectrum produced by the generating machine.

The duration of the shock was set to 20 ms, with a frequency content in the range between 100 Hz and 4 kHz, as shown in figure 17 in terms of standard shock response spectrum (SRS). The SRS is the acceleration spectrum that would result from applying the same shock to a damped harmonic oscillator with quality factor $Q = 10$.

2026 JINST 21 P11009

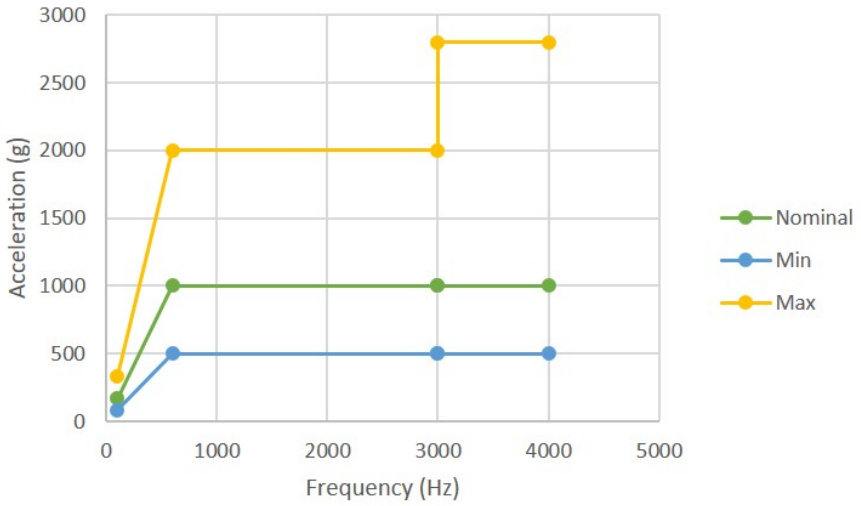

Figure 17. Shock response spectrum required to be injected at HEPD-02 base plate for pyroshock test on QM. The graph shows the nominal value and the allowed tolerance range for peak acceleration. The applied stimulus was also required to be higher than the nominal value for at least 50% of the frequency range.

The application of the desired shock spectrum required a multi-step preliminary calibration of the stimulus, to take into account the mechanical response of the actual HEPD-02 structure, significantly varying according to the fabrication tolerances of the real object. The STM (introduced in subsection 5.1) was used for the initial coarse calibration; the residual fine calibration and then the test were performed on the QM, thus greatly reducing the risk of overstressing the unit. For the same reason, the test was not carried out on FM.

After pyroshock, the vibration test verified the resistance to the continuous vibrational stimuli expected during launch and flight maneuvers. The test was carried out with a TIRA GmbH shaker system. For each of the three axes, a sinusoidal stimulus was applied, with a frequency sweep in the range between 10 and 100 Hz and levels shown in figure 18. This was followed by a sustained stimulus obtained by randomly combining frequency components in the range between 10 Hz and 2 kHz. The injected power spectral density (PSD) is shown in figure 19, resulting in an effective RMS acceleration of 7.55 g for FM and 11.3 g for QM.

The monitoring of acceleration values inside the HEPD-02 structure was made available by means of triaxial integrated-circuit piezoelectric accelerometers (PCB Piezotronics ICP 356A02), permanently installed in critical points (see figure 20). These sensors were read-out during the application of vibrational stimuli, through a service panel on the rear wall of HEPD-02.

The test success was evaluated after the application of the pyroshock or vibrational stimuli along each axis. The complete and correct operation of the detectors and electronics was verified. Searches for mechanical resonances were performed, by applying a low-level (0.5 g) sinusoidal acceleration with frequency sweep in the range between 10 Hz and 2.0 kHz. The searches showed the absence of unwanted resonance peaks under 100 Hz. In addition, the characteristic resonances of the structure at higher frequencies were found to be stable, with peak frequency variations within ±10% and peak acceleration variation within ±1 g. This meant that no permanent strains, fractures or detachments occurred.

2026 JINST 21 P11009

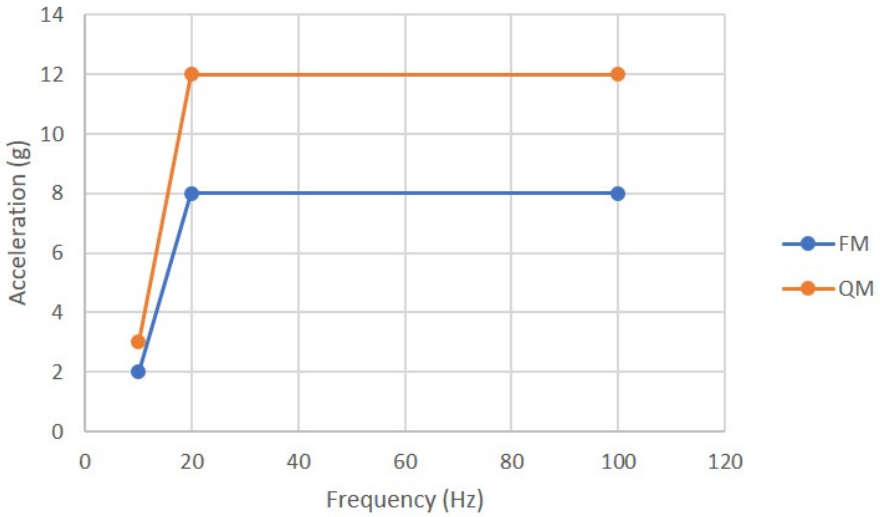

Figure 18. Peak acceleration injected at HEPD-02 base plate for sinusoidal stimulus on FM and QM. Tolerance range: ±10%. Frequency sweep rate: 4 octaves/minute for FM, 2 octaves/minute for QM.

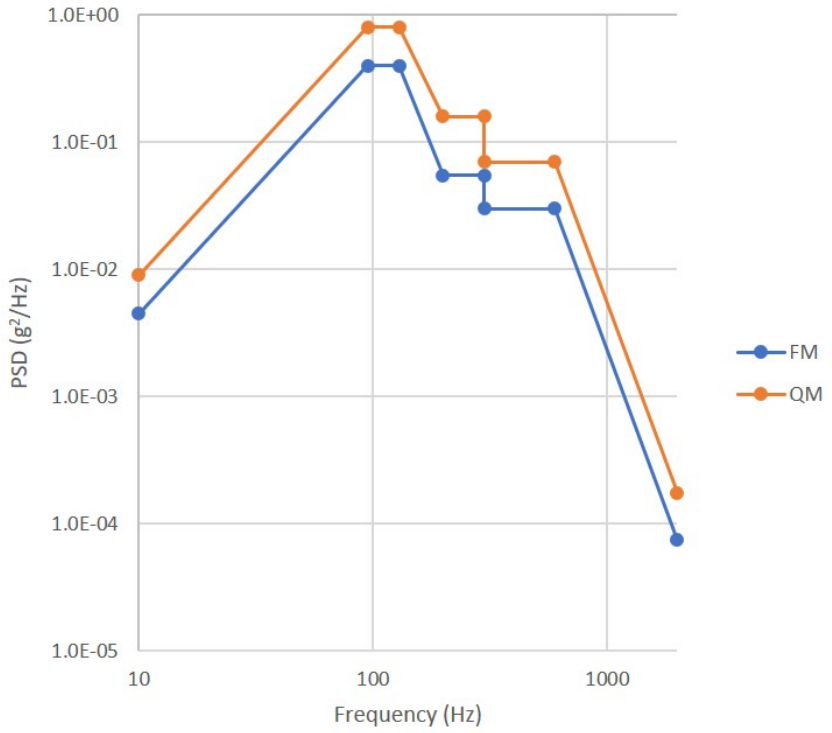

Figure 19. Power spectral density injected at HEPD-02 base plate for random stimulus on FM and QM. Tolerance range: ±1.5 dB below 1 kHz, ±3 dB above 1 kHz. Duration of applied stimulus: 1 min for FM, 2 min for QM.

2026 JINST 21 P11009

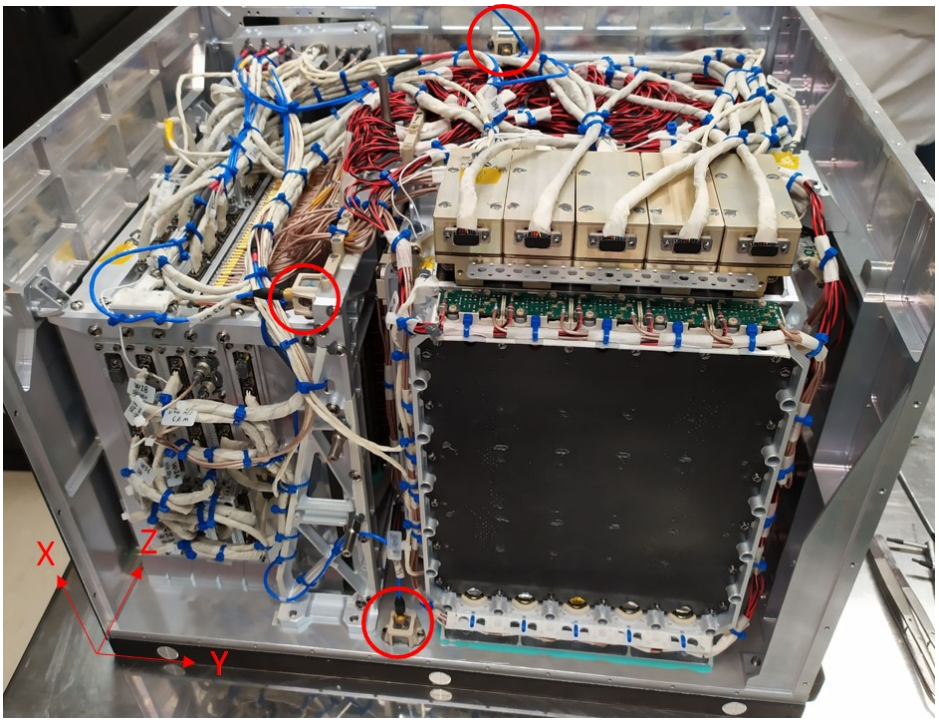

Figure 20. Picture of HEPD-02 QM during assembly, with indication of the 3 internal accelerometers.

6.2 Thermal and vacuum tests

The system-level thermal and vacuum tests were designed to verify the ability of HEPD-02 to operate for a long time in a much wider temperature range than specified in the operational requirements (−10 °C to +35 °C). The tests were carried out in air and under the vacuum conditions foreseen during flight, with repeated cycling between two extreme temperature points. In addition, these tests were aimed at the identification of possible early failures of defective parts by sustained thermal stresses and allowed verification of the absence of discharges in high-voltage circuits under vacuum conditions.

Table 4 reports the main specifications of the tests, which took place in the SERMS laboratory already mentioned in subsection 6.1. Temperature cycles were performed first in air at ambient pressure in a climatic chamber (Angelantoni DM1000 C15 ESS) and then in a vacuum chamber (Angelantoni HVT 2000). The cumulative duration of the cycles was 24 days for the FM and 38 days for the QM, evenly divided between the main and spare sides of the apparatus.

The sequence of applied temperature cycles is outlined in figure 21, starting with an increase to maximum temperature and ending with a decrease to ambient temperature, thus producing a semi-integer number of cycles. Starting with a temperature increase immediately brings the apparatus in the most challenging configuration, with the thermal gradients along the structure summing up to the increased base plate temperature; moreover, in vacuum condition the outgassing from materials is enhanced by the higher temperatures, thus creating an initial worst-case test environment. The last half cycle at high temperatures allows the return to ambient condition without the unwanted deposition on the equipment surfaces of humidity in air, or of previously outgassed volatile substances in vacuum.

The correct operation of HEPD-02 was verified during each temperature ramp and during dwell at the maximum and minimum cycle temperatures, where repeated power-on tests were also performed.

2026 JINST 21 P11009

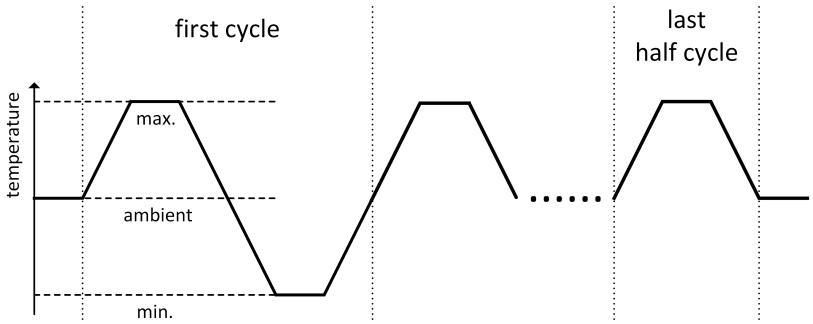

Figure 21. Schematic view of the temperature cycles performed during thermal and vacuum tests.

Table 4. Main characteristics of thermal and vacuum tests.

Condition		QM	FM
Min. base plate temperature (tolerance −4 °C, +0°C)		−30°C	−20°C
Max. base plate temperature (tolerance −0°C, +4°C)		+50°C	+45°C
Dwell time at max./min. temperature		> 4 h	
Air	Number of cycles	25.5	14.5
	Total duration	28 days	16 days
	Pressure	ambient	
Vacuum	Number of cycles	6.5	3.5
	Total duration	10 days	8 days
	Pressure	< 6.65 mPa	

HEPD-02 is equipped with > 120 internal thermal sensors installed throughout the structure. Of these, 6 sensors are positioned on each tracker stave and 10 sensors are mounted on the boards of the electronics assembly, for a close monitoring of the hottest parts of the apparatus. A subset of 7 sensors distributed in various mechanical frames was read-out directly by the chamber control system, through the HEPD-02 service panel; this allowed real-time internal temperature mapping during the tests.

The sensors showed that the thermal gradients along the structure were limited to ∼ 10 °C above the base plate temperature for the frames and to a few degrees more for the boards (figure 22). These results confirmed the predictions of the thermal design simulations and allowed them to be fine-tuned.

6.3 Electromagnetic compatibility (EMC) tests

These tests were aimed at verifying the electromagnetic compatibility of the HEPD-02 apparatus with operation on board the CSES-02 satellite. The susceptibility of HEPD-02 to the interference signals produced by the rest of the on-board equipment was considered, as well as the potential disturbances for other parts of the satellite due to the emissions of HEPD-02.

The measurements listed in table 5 were carried out on HEPD-02 FM, according to the requirements of DFH Satellite Co., the manufacturer of CSES-02. The tests are defined according to the NASA technical standard MSFC-SPEC-521C integrated by the engineering standard MIL-STD-461. The

2026 JINST 21 P11009

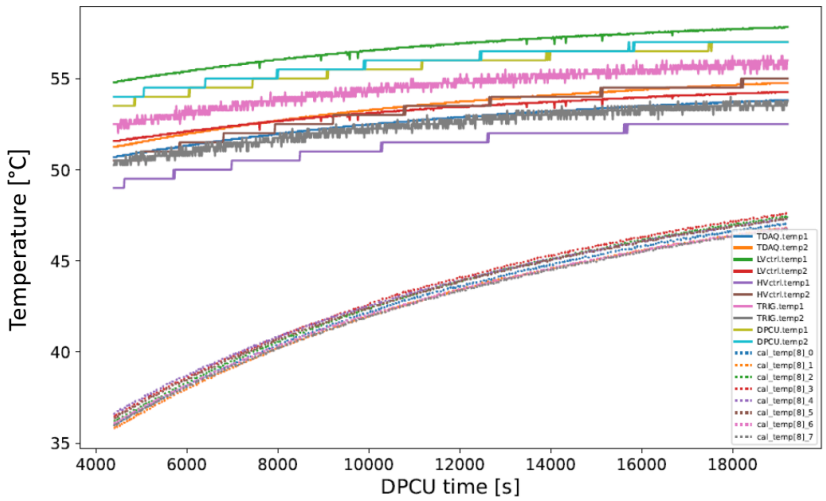

Figure 22. Temperatures of internal sensors mounted on boards (top group) and on RAN scintillator frames (bottom group) during dwell of FM at maximum cycle temperature in vacuum.

specifications are customized to match the peculiar characteristics of HEPD-02 and CSES-02. The interference interactions are indicated as conducted in the case of capacitive or inductive coupling on the cables connecting HEPD-02 with the satellite, as radiated in the case of coupling of the whole HEPD-02 structure through electromagnetic fields.

Table 5. List of EMC tests, classified according to NASA standard MSFC-SPEC-521C. More restrictive custom emission thresholds were applied to RE102 test in the range between 0.6 GHz and 1.6 GHz, to take into account the specific characteristics of CSES-02 satellite (see figure 32).

Test	Description	Frequency range
CS101	Conducted susceptibility of power bus input	30 Hz to 150 kHz
CS114	Conducted susceptibility of external cables and power bus input	10 kHz to 200 MHz
RS103	Radiated susceptibility	10 kHz to 18 GHz
CE102	Conducted emissions of power bus input	150 kHz to 10 MHz
RE102	Radiated emissions	200 MHz to 2 GHz

The test campaign took place at the Institute of Applied Physics "Nello Carrara" (IFAC) of the National Research Council (CNR) in Florence, Italy. A fully-anechoic shielded chamber was made available, with effective electromagnetic absorption up to 18 GHz, obtained with hybrid pyramidal absorbers installed on ferrite tiles of 10 mm thickness.

6.3.1 Susceptibility tests

The susceptibility tests CS101, CS114 and RS103 (see table 5) required the injection of a sinusoidal interference signal, with frequency varied according to a discrete-step sweep in the range of interest.

2026 JINST 21 P11009

The CS101 test studied the susceptibility to voltage disturbances conducted on the power bus, in the frequency range between 30 Hz and 150 kHz, according to the levels shown in figure 23. The stimulus was injected through a coupling transformer with the secondary coil inserted in the power input line and monitored by an oscilloscope, as illustrated in figure 24.

A line impedance stabilization network (LISN) was used to prevent disturbances from reaching the EGSE power supply. The LISN is a standard passive network, defined according to the MIL-STD-461 specifications.

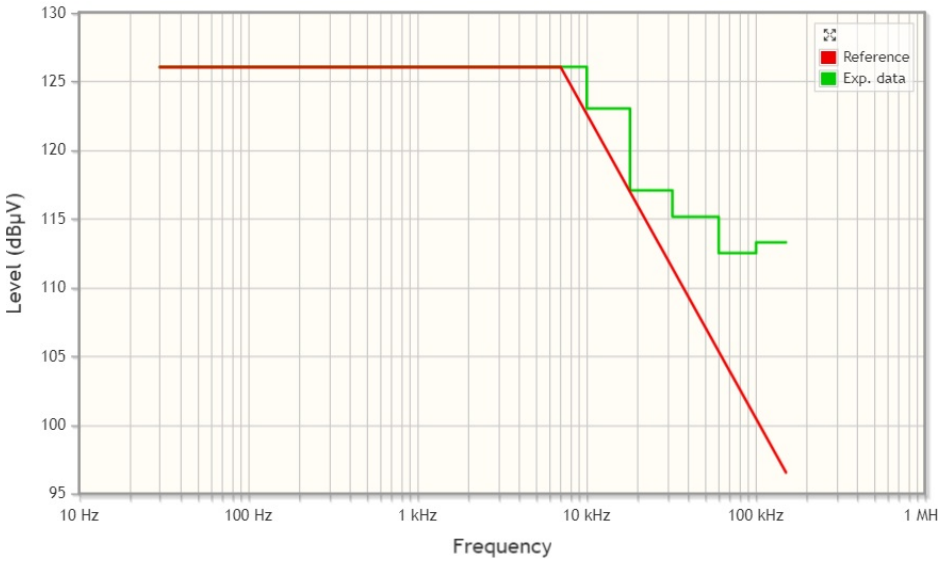

Figure 23. CS101 test: minimum required voltage stimulus (reference, red line). Also shown the minimum experimentally injected signal, when different (green line). The levels are expressed as RMS value of the sinusoidal signal; above 10 kHz, a 1 kHz pulse modulation is superimposed.

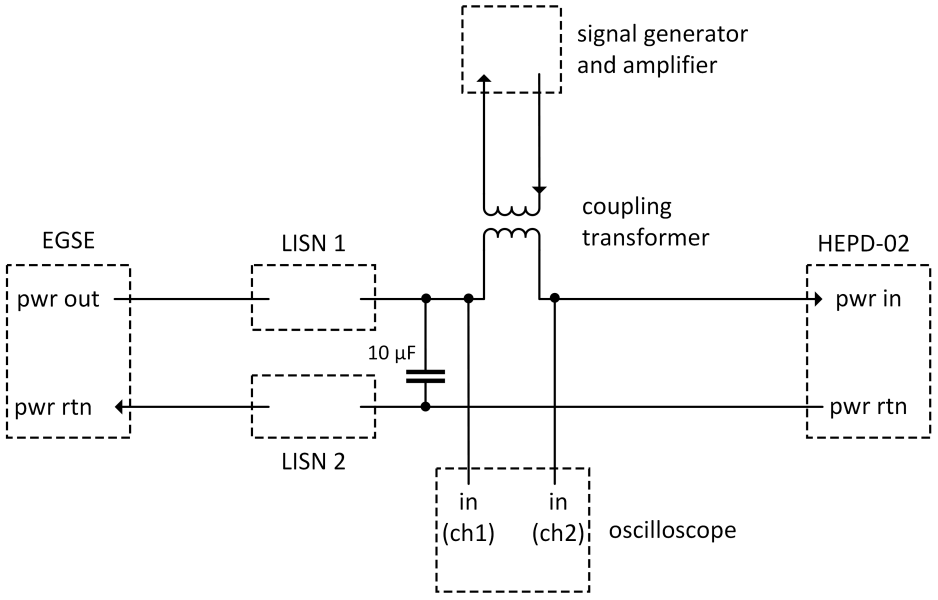

Figure 24. CS101 test: circuit set-up.

2026 JINST 21 P11009

The CS114 test was aimed at determining the susceptibility to current disturbances conducted on the loops formed by the cables and the chassis connections between HEPD-02 and CSES-02, in the frequency range between 10 kHz and 200 MHz. The test was executed for various possible coupling configurations, with a current injection probe surrounding one or more cables or groups of wires and generating a magnetic field that crossed the loop.

As an example, the case of the probe surrounding a single cable is shown in figure 25, with the corresponding stimulus levels in figure 26. The injected current was monitored by measuring the voltage across a calibrated resistor inserted in the cable screen.

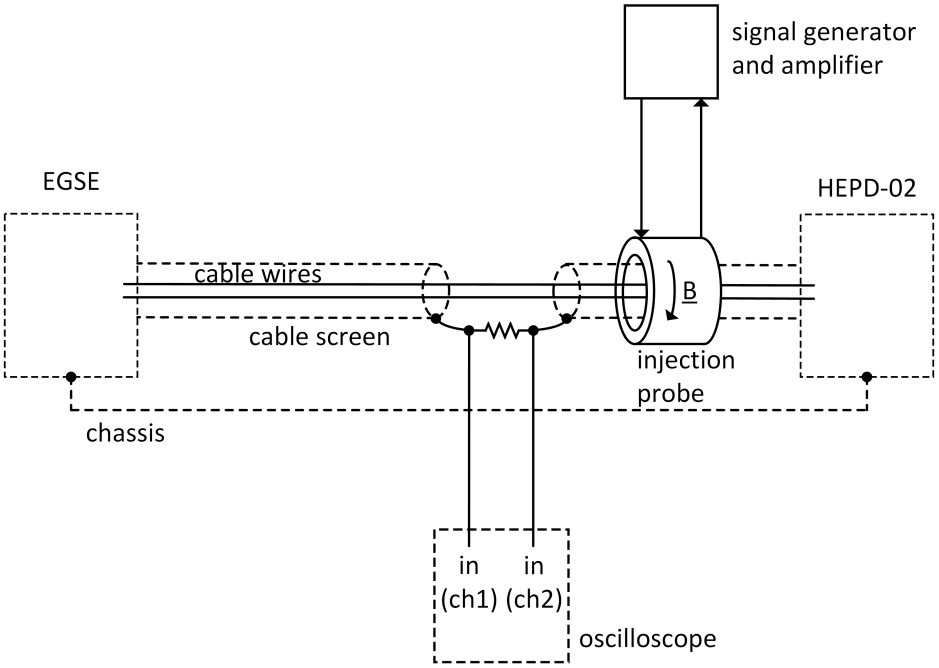

Figure 25. CS114 test: example of circuit set-up.

Finally, the RS103 test studied the susceptibility to electromagnetic disturbances radiated in the frequency range between 10 kHz and 18 GHz. The stimulus was injected through commercial antennas with appropriate transmission efficiency in each frequency sub-range above 30 MHz, with the typical set-up shown in figure 28. Below 30 MHz, a custom antenna was used, composed of two square metal grids (1 m × 1 m) vertically separated by 1 m and with HEPD-02 positioned between them.

Above 30 MHz, the measurement was performed twice, with the antenna positioned to produce a vertical or horizontal polarized electric field, according to the levels in figure 27. The amplitude of the injected signal was locally verified by positioning an electric field probe.

For all of the above mentioned tests, the correct operation of HEPD-02 was verified both during and after interference injection, finding acceptable noise levels in the detector signal and no functional anomalies, with the exception of one case of susceptibility. This was found during the CS114 test, with the current injection probe surrounding the cable carrying power and single-line telecommands/telemetries and with stimulus in the frequency range between 20 and 80 MHz.

Specifically, the disturbances generated spurious acquisition triggers with a rate of ~ 200 Hz, of the same order as the rates due to the incoming particles during flight. Under different interference conditions, the spurious trigger rate was at least 100 times smaller and therefore negligible. A

2026 JINST 21 P11009

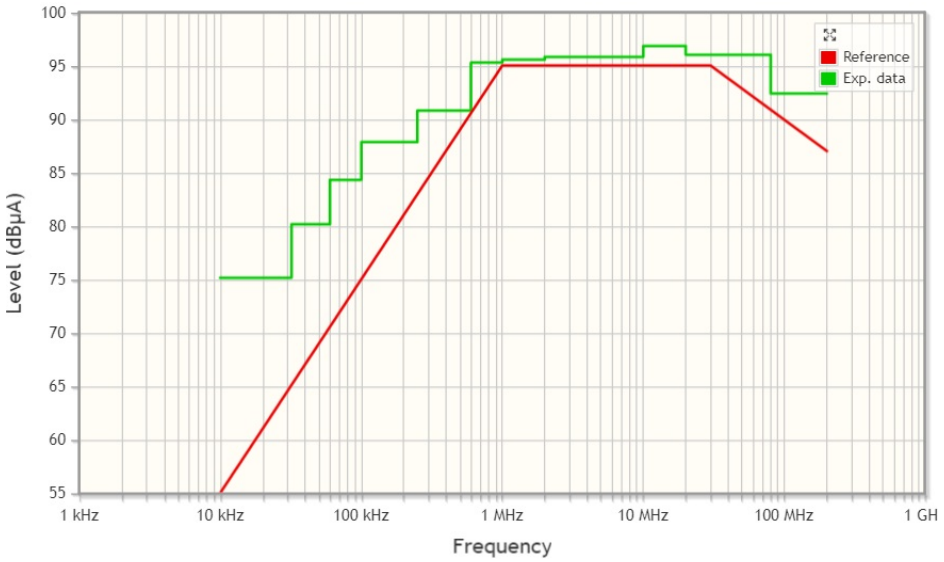

Figure 26. CS114 test: minimum required current stimulus (reference, red line) for the circuit set-up shown in figure 25. Also shown the minimum experimentally injected signal, when different (green line). The levels are expressed as RMS value of the sinusoidal signal; a 1 kHz pulse modulation is superimposed.

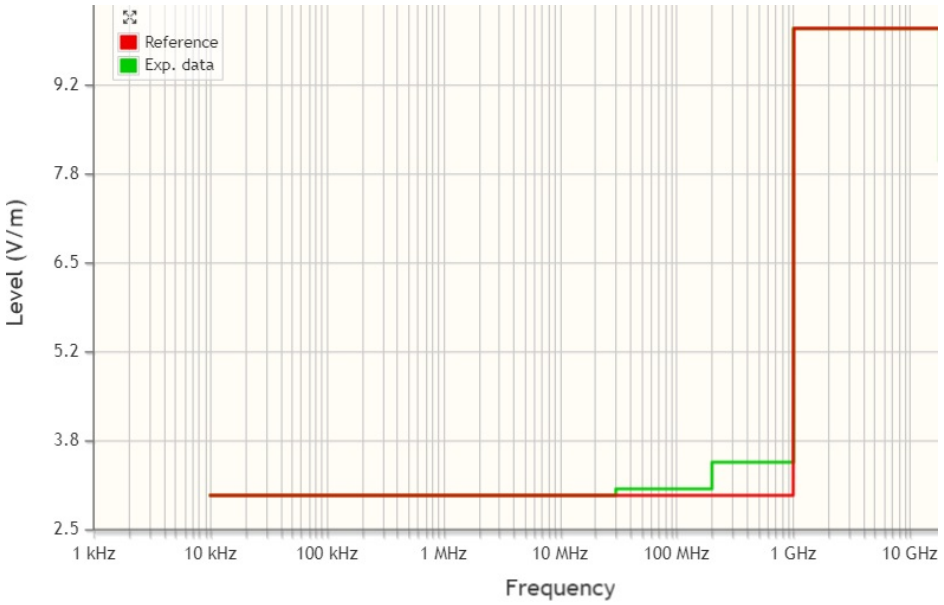

Figure 27. RS103 test: minimum required electric field stimulus (reference, red line). Also shown the minimum experimentally injected signal, when different, for the case of vertical polarization (green line). The levels are expressed as RMS value of the sinusoidal signal; a 1 kHz pulse modulation is superimposed.

2026 JINST 21 P11009



Figure 28. Typical set-up during RS103 test, here employing the ARA DRG-118/A antenna.

susceptibility threshold of 8 mA RMS injected current was determined by reducing the interference signal amplitude until the effect disappeared. Subsequent analysis showed that the actual interference signal to be found on board the CSES-02 satellite would be much smaller than the susceptibility threshold, and therefore no such interference effect was expected. In fact, this prediction was later confirmed during satellite-level tests.

6.3.2 Emission tests

The CE102 and RE102 emission tests (see table 5) required HEPD-02 to operate while a discrete frequency scan of electromagnetic emissions was conducted with a spectrum analyzer.

The CE102 test measured the emissions conducted on the power bus input line and return line separately, in the frequency range between 150 kHz and 10 MHz, according to the set-up shown in figure 29. The LISN allowed the extraction of the interference signal injected by HEPD-02 on the power line, while removing the unwanted contribution from the EGSE power supply.

The RE102 test studied the emissions of HEPD-02 radiated in the frequency range between 200 MHz and 2 GHz, with the set-up shown in figure 30. The electric field was measured with a double ridged horn antenna. The measurement was repeated with the antenna rotated by 90° to detect the vertical and horizontal polarization components.

Examples of the measured emission spectra are reported in figures 31 and 32. The figures also show the reference thresholds for acceptable maximum emissions, which were defined to be conservatively lower than the susceptibility thresholds expected for the satellite structure and the other payloads. This approach was required because at the time of the HEPD-02 emission tests the actual susceptibility of the rest of the CSES-02 equipment was not yet accurately determined.

In some cases, the emissions turned out to be higher than the reference thresholds, as can be seen in figure 32. These emission levels were later compared by DFH Satellite Co. with the susceptibility thresholds of the satellite structure and of the other payloads once those values were available. The comparisons showed that the HEPD-02 emissions were fully acceptable; subsequently, this conclusion was experimentally confirmed with satellite-level tests.

2026 JINST 21 P11009

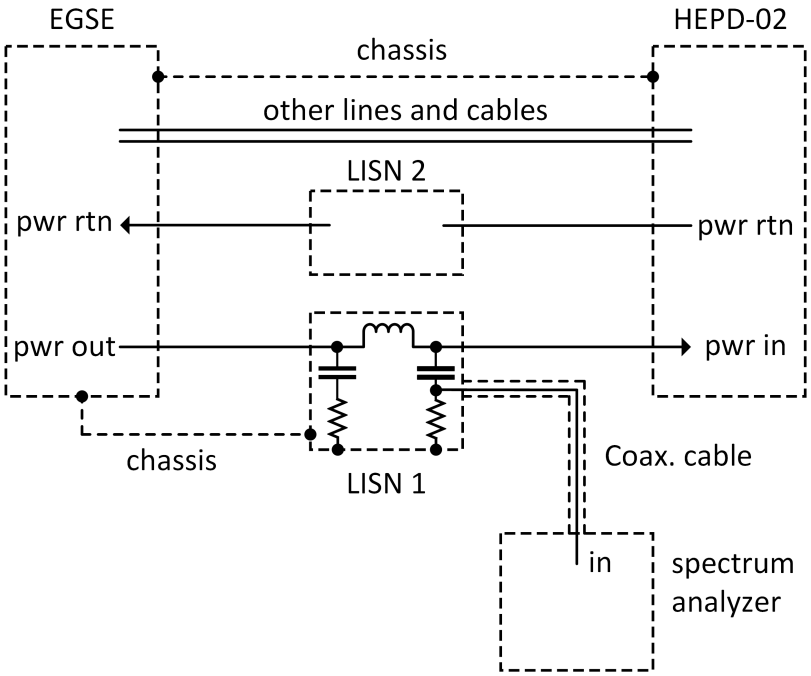

Figure 29. CE102 test: circuit set-up for extraction of emitted signal from LISN 1 on power bus input line. LISN 2 is used for signal extraction on power return line.

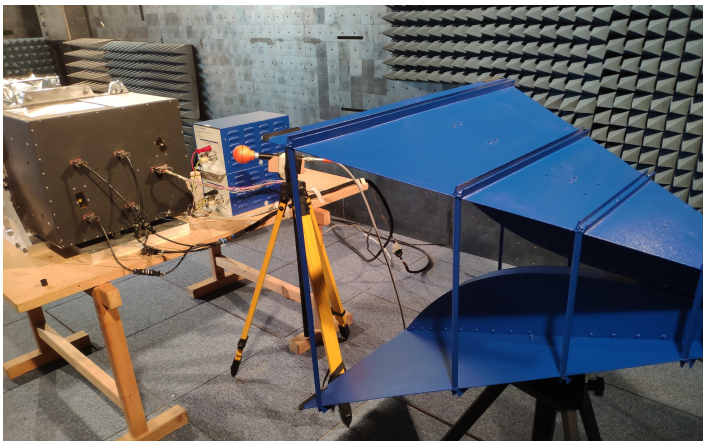

Figure 30. RE102 test: picture of antenna set-up. The antenna opening is 69.0 cm × 94.5 cm.

7 Conclusions

HEPD-02 FM was shipped to DFH Satellite Co. (China) in January 2024 for installation on board the CSES-02 satellite.

The fully assembled satellite underwent a sequence of functional and environmental tests between February 2024 and February 2025. These included mechanical stresses, emulation of thermal flight conditions with directional heating by the Sun, thermal cycling, and sustained continuous operation for 5 days. The tests confirmed operation stability and the absence of anomalous behaviours for both the main and spare sides of HEPD-02.

2026 JINST 21 P11009

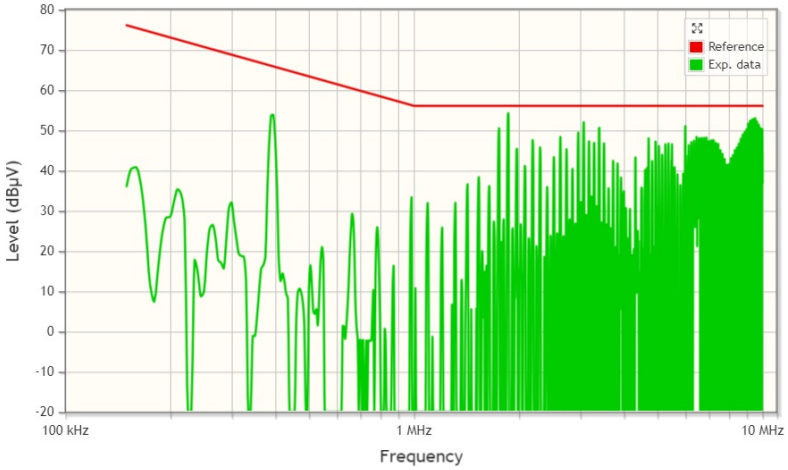

Figure 31. CE102 test: measured HEPD-02 main-side voltage emission spectrum on power bus input, after correction for LISN transfer function. The reference attention threshold is superimposed.

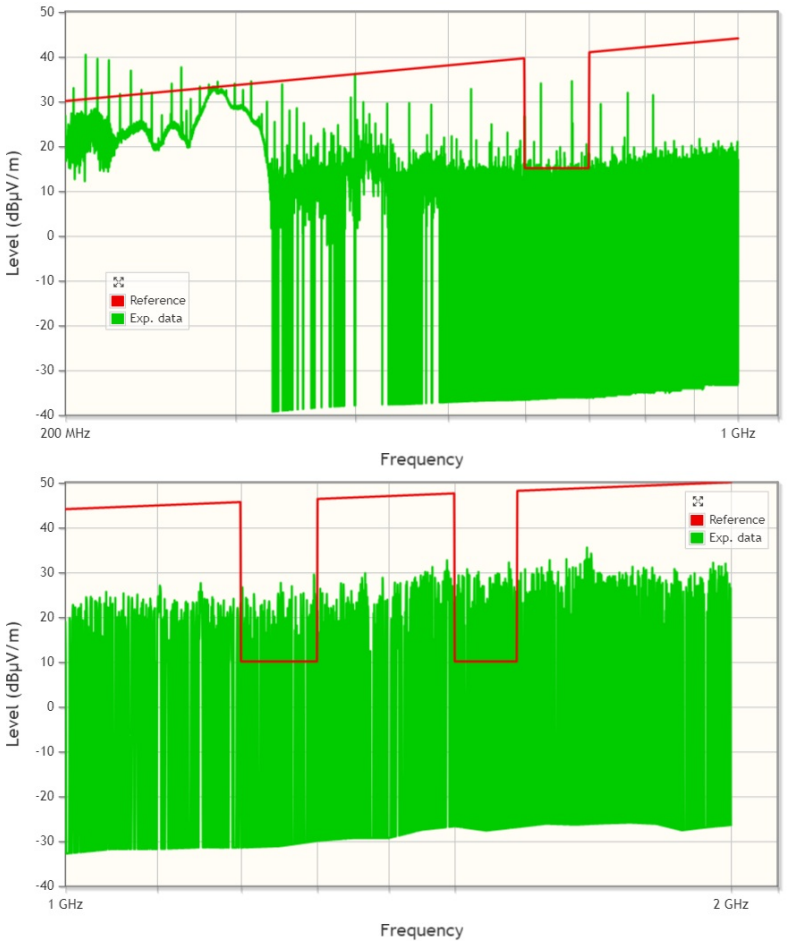

Figure 32. RE102 test: measured HEPD-02 main-side emission spectrum for vertical electric-field polarization, after correction for antenna transfer function. The reference attention threshold is superimposed. In the frequency ranges between 0.6 and 0.7 GHz, 1.2 and 1.3 GHz, 1.5 and 1.6 GHz, more restrictive threshold levels than RE102 ones were applied to take into account the specific characteristics of CSES-02 satellite.

2026 JINST 21 P11009

In May 2025, CSES-02 was transported to Jiuquan Satellite Launch Center (JSLC) located across Ejin Banner, Inner Mongolia, and Jinta County, Gansu (China) and installed on the Long March 2D launch vehicle. The satellite was launched on 14 June 2025.

On 20 June, the main side of HEPD-02 was powered on and the specific health check procedures were successfully performed. A commissioning phase followed until the end of December 2025 to verify the correct operation and to set up and adjust the configuration of the detectors according to the actual in-flight environment. During this phase, both the main and the spare sides of the apparatus were tested and calibrated.

After successful completion of the commissioning, HEPD-02 was set to its normal, fully automatic operation mode to continuously deliver scientific data.

Acknowledgments

This work was supported by the Italian Space Agency (ASI) in the framework of the "Accordo attuativo 2019-22-HH.0 Programma Limadou-2 attività di fase B2/C/D/E1" and the ASI-INFN agreement n. 2021-43-HH.0.

The authors gratefully acknowledge the staff of the SERMS Laboratory and the INFN Section of Perugia for their support and for providing the facilities and instrumentation used during the qualification and acceptance tests of HEPD-02.

References

[1] X.H. Shen et al., *The state-of-the-art of the China Seismo-Electromagnetic Satellite mission*, *Sci. China Technol. Sci.* **61** (2018) 634.

[2] O. Molchanov et al., *Global diagnostics of the ionospheric perturbations related to the seismic activity using the VLF radio signals collected on the DEMETER satellite*, *Nat. Hazards Earth Syst. Sci.* **6** (2006) 745.

[3] Z. Zhima et al., *Storm-Time Features of the Ionospheric ELF/VLF Waves and Energetic Electron Fluxes Revealed by the China Seismo-Electromagnetic Satellite*, *Appl. Sci.* **11** (2021) 2617.

[4] S. Bartocci et al., *Galactic Cosmic-Ray Hydrogen Spectra in the 40–250 MeV Range Measured by the High-energy Particle Detector (HEPD) on board the CSES-01 Satellite between 2018 and 2020*, *Astrophys. J.* **901** (2020) 8.

[5] P. Picozza et al., *Scientific Goals and In-orbit Performance of the High-energy Particle Detector on Board the CSES*, *Astrophys. J. Suppl.* **243** (2019) 16.

[6] S. Bartocci et al., *The High-Energy Particle Detector on Board the CSES-02 Satellite*, *Space Sci. Rev.* **222** (2026) 26.

[7] E.C. Stone et al., *Voyager 1 Observes Low-Energy Galactic Cosmic Rays in a Region Depleted of Heliospheric Ions*, *Science* **341** (2013) 1236408.

[8] E.C. Stone, A.C. Cummings, B.C. Heikkila and N. Lal, *Cosmic ray measurements from Voyager 2 as it crossed into interstellar space*, *Nature Astron.* **3** (2019) 1013.

[9] AMS collaboration, *The Alpha Magnetic Spectrometer (AMS) on the international space station: Part II — Results from the first seven years*, *Phys. Rept.* **894** (2021) 1.

[10] P. Picozza et al., *PAMELA: A Payload for Antimatter Matter Exploration and Light-nuclei Astrophysics*, *Astropart. Phys.* **27** (2007) 296 [astro-ph/0608697].

2026 JINST 21 P11009

[11] C. Fidani, R. Battiston and W.J. Burger, *A Study of the Correlation between Earthquakes and NOAA Satellite Energetic Particle Bursts*, *Remote Sens.* **2** (2010) 2170.

[12] S. Bartocci et al., *The Scintillation Counters of the High-Energy Particle Detector of the China Seismo-Electromagnetic (CSES-02) Satellite*, *Remote Sens.* **16** (2024) 3982.

[13] L. Barioglio et al., *The Monolithic Active Pixel Sensors Tracker System of the High-Energy Particle Detector Aboard the Second Chinese Seismo-Electromagnetic Satellite*, *IEEE Aerosp. Electron. Syst. Mag.* **40** (2025) 28.

[14] ALICE collaboration, *The ALPIDE pixel sensor chip for the upgrade of the ALICE Inner Tracking System*, *Nucl. Instrum. Meth. A* **845** (2017) 583.

[15] G. Ambrosi et al., *The electronics of the High-Energy Particle Detector on board the CSES-01 satellite*, *Nucl. Instrum. Meth. A* **1013** (2021) 165639.

[16] A. Anastasio et al., *Trigger and Calorimeter Data Acquisition of the High-Energy Particle Detector Onboard the CSES-02 Satellite*, *IEEE Trans. Instrum. Measur.* **74** (2025) 2008413.

[17] S. Bartocci et al., *Control and read-out of the HEPD-02 tracking system onboard CSES-02 satellite*, 2026 *JINST* **21** P01030 [arXiv:2512.23885].

[18] L. Ruckman, *Spacewire light*, DOI:10.11578/dc.20220810.1.

[19] S. Bartocci et al., *Development of the power supply of HEPD-02 instrument on board CSES-02 satellite*, 2025 *JINST* **20** P06005.

[20] S. Coli et al., *Thermo-mechanical design for ALPIDE pixel sensor chip in a high-energy particle detector space module*, 2022 *JINST* **17** C01019.

2026 JINST 21 P11009